Recursive Algorithms for the Estimation of Multiple Superimposed Undamped Tones and Their Application to Radar Systems

PASQUALE DI VIESTI (10), Student Member, IEEE

ALESSANDRO DAVOLI (10), Student Member, IEEE

GIORGIO GUERZONI (10)

GIORGIO M. VITETTA (10), Senior Member, IEEE

University of Modena and Reggio Emilia, Modena, Italy

Consorzio Nazionale Interuniversitario per le Telecomunicazioni, Parma, Italy

In this article, two recursive algorithms for the detection of multiple superimposed tones in noise and the estimation of their parameters are derived. They are based on a maximum likelihood approach and combine an innovative single-tone estimator with a serial cancellation procedure. Our numerical results lead to the conclusion that the developed methods can achieve a substantially better accuracy-complexity tradeoff than various related techniques in the presence of multiple closely spaced tones. Moreover, they can be exploited to detect multiple closely spaced targets and estimate their spatial coordinates in multiple-input multiple-output frequency-modulated continuous wave radar systems.

Manuscript received 9 December 2021; revised 26 May 2022 and 22 August 2022; accepted 8 September 2022. Date of publication 13 September 2022; date of current version 12 April 2023.

DOI. No. 10.1109/TAES.2022.3206176

Refereeing of this contribution was handled by R. S. Adve.

This work was supported in part by CNH Industrial Italia S.p.A. and in part by CNH Industrial Belgium NV.

Authors' addresses: The authors are with the Department of Engineering "Enzo Ferrari," University of Modena and Reggio Emilia, 41125 Modena, Italy, and also with the Consorzio Nazionale Interuniversitario per le Telecomunicazioni, 43124 Parma, Italy, E-mail: (pasquale.diviesti@unimore.it; alessandro.davoli@unimore.it; giorgio.guerzoni@unimore.it; giorgio.vitetta@unimore.it). (Corresponding author: Pasquale Di Viesti.)

This work is licensed under a Creative Commons Attribution 4.0 License. For more information, see https://creativecommons.org/licenses/by/4.0/

I. INTRODUCTION

The problem of estimating the amplitude, phase, and frequency of multiple (say L) tones in additive white Gaussian noise (AWGN) has received significant attention for a number of years because of its relevance in various fields, including radar systems and wireless communications (see, e.g., [1], [2], [3], and [4], respectively). It is well known that the maximum likelihood (ML) approach to this problem leads to a complicated nonlinear optimization problem. Substantial simplifications can be made when the L tone frequencies are sufficiently well separated and the number N of available signal samples is large enough [5], [6], [7]. In fact, under these assumptions, each tone has a limited influence on the estimation of the others, so that approximate ML estimation can be achieved through a conceptually simple sequential procedure that consists in iteratively executing two steps [6]. In the first step of this procedure, the parameters of the dominant tone (i.e., of the tone associated with the largest peak in the periodogram of the observed signal) are estimated in an ML fashion. In its second step, instead, the estimated tone is subtracted from the available signal samples, and a new periodogram is computed for the resulting residual. These steps are repeated until all the detectable tones are estimated. The technical relevance of this procedure is motivated by the following relevant advantages [8].

- 1) It turns a complicated multidimensional problem (whose dimensionality is usually unknown a priori) into a sequence of lower dimensional subproblems. Consequently, its overall complexity is proportional to that required to solve each of such subproblems and is usually much lower than that of *parametric estimation methods* (e.g., the MUSIC [9] and the ESPRIT [10]) and *nonparametric spectral estimators* (e.g., the Capon method [11], the APES [12], and the IAA-APES [13]).
- 2) It performs better than independently estimating the tones associated with the largest peaks of the original periodogram. In fact, it allows us to identify peaks that are initially masked by the leakage due to nearby tones.
- 3) It is able to estimate an unknown *L* in a simple fashion. In fact, this result can be achieved setting the initial value of this parameter to zero and applying a suitable test to establish whether, at each repetition of its first step, the largest peak detected in the periodogram of the last residual is significant [5] or whether, at each repetition of its second step, the energy of the new residual is large enough [14]. If one of these conditions is satisfied, the estimate of *L* is incremented by one and the next step is carried out; otherwise, the estimation process is terminated. It is worth stressing that various estimation methods (e.g., the MUSIC and the ESPRIT) require the prior knowledge of *L* and that, in these cases, the use of

some methods, such as the generalized *Akaike information criterion* [15] or the *minimum description length* [16], is commonly proposed for the estimation of this parameter; however, the computational effort they require is not negligible.

The three-step procedure described above, despite its advantages, suffers from the following two shortcomings.

- Inaccuracies in the estimation of each tone accomplished in its first step result in an imperfect cancellation of the tone itself and, thus, in *error accumulation*; the intensity of this phenomenon increases with iterations, affecting the estimation accuracy of the weakest tones.
- 2) The estimate of each tone is potentially biased, because of the presence of other tones [7]. Biases are influenced by the relative phase, frequency, and amplitude of the superimposed tones and are expected to be more relevant in the first estimated frequencies, since these suffer from stronger interference from other tones. For this reason, the overall accuracy of this procedure depends on that of the employed single-tone estimator and can be improved by adopting specific methods for mitigating the estimation bias. As far as the first issue is concerned, it is important to point out that the optimal (i.e., ML) estimation of a single tone in AWGN is a computationally hard task. This is mainly due to the fact that the ML metric is a highly nonlinear function that does not lend itself to easy maximization (see, e.g., [17]). In practice, the most accurate ML-based single-tone estimators available in the technical literature achieve an approximate maximization of this metric through a two-step procedure; the first step consists in a coarse search of tone frequency, whereas the second one in a fine estimation generating an estimate of the so-called frequency residual (i.e., of the difference between the real frequency and its coarse estimate). Coarse estimation is always based on the maximization of the periodogram of the observed signal, whereas fine estimation can be accomplished in an open-loop fashion or through an iterative procedure. On the one hand, all the open-loop estimators exploit spectral interpolation to infer the frequency residual from the analysis of the fast Fourier transform (FFT) coefficients at the maxima of the associated periodogram and at frequencies adjacent to it [8], [18], [19], [20], [21], [22], [23], [24], [25], [26], [27]. Unfortunately, unlike iterative estimators, the accuracy they achieve is frequency dependent and gets smaller when the signal frequency approaches the center of one of the FFT bins. On the other hand, the iterative estimation techniques available in the technical literature are based on various methods, namely:
 - a) standard numerical methods for locating the global maximum of a function (e.g., the secant method [28] or the Newton's method [29]);

- b) an iterative method for binary search, known as the *dichotomous search of the periodogram peak* [30], [31];
- c) interpolation methods amenable to iterative implementation [32], [33], [34], [35], [36], [37];
- d) the combination of the above-mentioned dichotomous search with various interpolation techniques [38];
- e) the computation of the first derivative of the spectrum [39].

The use of some of these algorithms in multiple-tone estimators based on the above-mentioned serial cancellation approach has been investigated in [8], [14], [15], [40], [41], [42], [43], and [44]. On the one hand, the periodogram-based (coarse) estimation method has been employed in the CLEAN algorithm [45], [46], [47], in the more CLEAN [14], and in the RELAX algorithm [15]. Note that, since a fine estimation step is missing in all these algorithms, achieving high accuracy requires the use of zero padding and of a large FFT order. On the other hand, the exploitation of more refined single-tone estimators has been investigated in [8], [40], [41], [42], and [44]. In particular, the use of open-loop interpolation methods exploiting three or five adjacent spectral coefficients (including the one associated with the coarse frequency estimate) has been studied in [8] and [44], whereas that of the iterative methods developed in [32] and [48] has been analyzed in [40], [41], and [42], respectively.

As far as the second technical issue (i.e., estimation bias) is concerned, it is worth mentioning that the most straightforward methods for bias mitigation rely on the use of 1) zero padding for enhancing periodogram spectral resolution and 2) window functions [7], [17], [49], [50], [51], [52]; the price to be paid for these choices is an increase in the overall computational cost and in the variance of computed estimates, respectively. More refined methods are represented by interpolators with intrinsic leakage rejection [8] and nonlinear optimization methods. The last class of methods includes the expectation-maximization (EM) algorithm [53], the space-alternating generalized EM algorithm [3], [54], the Newton's method [29], [55], and different optimization algorithms that employ cyclic cancellation procedures [14], [15], [42]. In the last case, tone re-estimation is accomplished after removing the interference of both the stronger and weaker tones as the iterations of the serial cancellation procedure evolve [14], [15] or after detecting and estimating the parameters of all tones [42]; the most refined version of the first method is described in [15], where tone re-estimation is iterated after the estimation of each new tone, to generate excellent initial estimates for the next step (i.e., for the estimation of the next tone). Tone re-estimation reduces error accumulation and leads to convergence to the ML solution in the absence of noise if the frequency spacing of the detected tones is large enough; however, this result is achieved at the price of an increase of the computational cost and latency [14].

This article aims at providing various new results about the estimation of multiple superimposed tones and their exploitation in colocated multiple-input multiple-output (MIMO) frequency-modulated continuous wave (FMCW) radar systems operating at millimeter waves (mmWaves) [56], [57]. Its contribution is threefold and can be summarized as follows:

- An ML-based estimator of a single complex tone is developed. This estimator is based on the periodogram method for coarse frequency estimation and on a new iterative algorithm for the estimation of the frequency residual and the complex amplitude. The last algorithm requires, unlike all the other related estimation methods available in the technical literature, the evaluation of multiple spectral coefficients. Moreover, its derivation is based on:
 - a) a new approximate expression of the ML metric;
 - b) the exploitation of the *alternating minimization* (AM) technique for the maximization of this metric (see, e.g., [58], Par. IV-A]).
- 2) Two recursive algorithms for the estimation of the parameters of multiple superimposed tones are derived. These algorithms combine the abovementioned single-tone estimator with a serial cancellation approach.
- 3) The accuracy of our single and multiple estimators is assessed by extensive computer simulations and compared with that achieved by all the other related algorithms available in the technical literature; both synthetically generated data and the measurements acquired through a commercial MIMO FMCW radar are processed.

Our numerical results lead to the following conclusions.

- 1) Our single-tone estimator performs similarly as other known estimators.
- 2) Our multiple-tone estimators outperform all the other related estimators in terms of the probability of convergence and achieve similar or better accuracy in the presence of arbitrary frequency residuals. Moreover, our multiple-tone estimators are able to reliably operate in the presence of multiple closely spaced tones, when all the other related estimators fail. For this reason, if employed in FMCW radar systems, they allow us to achieve a good spatial resolution in the presence of a dense distribution of point targets.

The rest of this article is organized as follows. In Section II, the employed signal model is defined. Section III is devoted to the derivation of our single- and multiple-tone estimation algorithms, to the assessment of their computational complexity, and to the analysis of their similarities and differences with related estimators available in the technical literature. In Section IV, the performance of our estimation algorithms is assessed and compared with that achieved by other estimators. Finally, Section V concludes this article.

Notations: $\Re\{x\}$ and $\Im\{x\}$ denote the real and imaginary parts of the complex variable x, respectively.

II. SIGNAL MODELS

In this article, we focus on the problem of estimating all the parameters of the complex sequence¹

$$x_n = \sum_{l=0}^{L-1} A_l \exp(j2\pi n F_l) + w_n$$
 (1)

with n = 0, 1,..., N - 1; here, A_l and $F_l \in [0, 1)$ denote the *complex amplitude* and the *normalized frequency*, respectively, of the lth complex tone appearing in the right-hand side (RHS) of (1). The last equation can also be rewritten as

$$x_n = \sum_{l=0}^{L-1} a_l \exp(j(2\pi nF_l + \psi_l)) + w_n$$
 (2)

where $a_l \triangleq |A_l|$, $\psi_l \triangleq \angle(A_l)$, w_n is the *n*th sample of an AWGN sequence (whose elements have zero mean and variance $2\sigma^2$), N is the overall number of samples, and $\angle(x)$ denote the phase of the complex quantity x.

The signal model (1) appears in a number of problems concerning biomedical applications, wireless communications, and radar systems. Our interest in the considered estimation problem has been motivated by its relevance in the last field and, in particular, in colocated MIMO FMCW radar systems operating at mmWave [1], [59].

III. APPROXIMATE MAXIMUM LIKELIHOOD ESTIMA-TION OF A SINGLE TONE AND OF MULTIPLE TONES

In this section, we first derive a new method for estimating the parameters of a complex tone. Then, we show how this method can be exploited to detect multiple superimposed tones and estimate their parameters through a deterministic procedure based on successive cancellations. Finally, we analyze the computational complexity of the developed estimation methods and compare them with related techniques available in the technical literature.

A. Estimation of a Single Tone

Let us focus on the problem of estimating the parameters (namely, the frequency and complex amplitude) of a single tone contained in the *complex* sequence $\{x_n; n = 0, 1,..., N-1\}$, whose nth sample is expressed by (1) with L=1, i.e., as

$$x_n = A \exp(j2\pi nF) + w_n \tag{3}$$

where A and F are the complex amplitude and the normalized frequency, respectively, of the tone itself. It is well known that the ML estimates $F_{\rm ML}$ and $A_{\rm ML}$ of the

¹Estimation methods have also been developed for the real counterpart of this model. Our main results can be found in [59].

parameters F and A, respectively, represent the solution of the *least-squares problem* (see, e.g., [28], (22)])

$$(F_{\mathrm{ML}}, A_{\mathrm{ML}}) \triangleq \arg\min_{\tilde{F}, \tilde{A}} \varepsilon(\tilde{F}, \tilde{A})$$
 (4)

where \tilde{F} and \tilde{A} represent trial values of F and A, respectively

$$\varepsilon(\tilde{F}, \tilde{A}) \triangleq \frac{1}{N} \sum_{n=0}^{N-1} \varepsilon_n(\tilde{F}, \tilde{A}). \tag{5}$$

is the mean square error (MSE) evaluated over the whole observation interval

$$\varepsilon_n(\tilde{F}, \tilde{A}) \triangleq \left| x_n - s_n(\tilde{F}, \tilde{A}) \right|^2$$
 (6)

is the *square error* between the noisy sample x_n (3) and its useful component $s_n(\tilde{F}, \tilde{A}) \triangleq \tilde{A} \exp(j2\pi n\tilde{F})$ evaluated under the assumption that $F = \tilde{F}$ and $A = \tilde{A}$. Substituting the RHS of the last expression into that of (6) yields

$$\varepsilon_n(\tilde{F}, \tilde{A}) = |x_n|^2 + |\tilde{A}|^2 - 2\Re\{x_n \tilde{A}^* \exp(-j2\pi n\tilde{F})\}.$$
 (7)

Then, substituting the RHS of (7) into that of (5) yields

$$\varepsilon(\tilde{F}, \tilde{A}) = \varepsilon_x + |\tilde{A}|^2 - 2\Re\{\tilde{A}^*\bar{X}(\tilde{F})\}$$
 (8)

where $\varepsilon_x \triangleq \sum_{n=0}^{N-1} |x_n|^2 / N$ and

$$\bar{X}(\tilde{F}) \triangleq \frac{1}{N} \sum_{n=0}^{N-1} x_n \exp(-j2\pi n\tilde{F})$$
 (9)

is, up to the scale factor 1/N, the *Fourier transform* of the sequence $\{x_n\}$.

Based on (8), it is not difficult to show that the optimization problem expressed by (4) does not admit a closed-form solution because of the nonlinear dependence of the function $\varepsilon(\tilde{F},\tilde{A})$ on its variable \tilde{F} . However, an approximate solution to this problem can be derived by:

- 1) exploiting an iterative method, known as AM (see, e.g., [58]). This allows us to transform the 2-D optimization problem expressed by (4) into a couple of interconnected 1-D problems, one involving the variable \tilde{F} only (conditioned on the knowledge of \tilde{A}), the other one involving the variable \tilde{A} only (conditioned on the knowledge of \tilde{F});
- 2) expressing the dependence of the function $\varepsilon(\tilde{F}, \tilde{A})$ on the variable \tilde{F} through the couple $(F_c, \tilde{\delta})$ such that

$$\tilde{F} = F_c + \tilde{\delta} F_{\rm DFT} \tag{10}$$

where F_c is a given *coarse estimate* of F, $\tilde{\delta}$ is a real variable called *residual* and belonging to the interval [-0.5, 0.5],

$$F_{\rm DFT} = 1/N_0 \tag{11}$$

is the normalized fundamental frequency associated with the N_0 th-order discrete Fourier transform (DFT)

$$\mathbf{X}_0 = \left[X_{0,0}, X_{0,1}, \dots, X_{0,N_0-1} \right]^T \tag{12}$$

of the zero-padded version

$$\mathbf{x}_{0,\text{ZP}} = \begin{bmatrix} \mathbf{x}_0^T \ \mathbf{0}_{(M-1)N}^T \end{bmatrix}^T \tag{13}$$

of the vector

$$\mathbf{x}_0 \triangleq \begin{bmatrix} x_0, x_1, \dots, x_{N-1} \end{bmatrix}^T \tag{14}$$

collecting all the elements of the sequence $\{x_n\}$, M is a positive integer (dubbed *oversampling factor*), $\mathbf{0}_D$ is a D-dimensional (column) null vector, and $N_0 \triangleq M \cdot N$.

3) expressing the dependence of the function $\varepsilon(\tilde{F}, \tilde{A})$ (8) on the variable $\tilde{\delta}$ through its powers $\{\tilde{\delta}^l; 0 \le l \le 3\}$; this result is achieved by approximating the complex exponential $\exp(-j2\pi n\tilde{\delta} F_{\rm DFT})$ appearing in the expression of $\varepsilon(\tilde{F}, \tilde{A})$ with its Taylor expansion truncated to a proper order (see below).

Let us show now how these principles can be put into practice. First of all, the exploitation of the above-mentioned AM approach requires solving the following two subproblems: **P1**) minimizing the cost function $\varepsilon(\tilde{F}, \tilde{A})$ (8) with respect to \tilde{A} , given $\tilde{F} = \hat{F}$; and **P2**) minimizing the same function with respect to \tilde{F} , given $\tilde{A} = \hat{A}$. Subproblem **P1** can be easily solved thanks to the polynomial dependence of the cost function $\varepsilon(\hat{F}, \tilde{A})$ on the variable \tilde{A} . In fact, the function $\varepsilon(\hat{F}, \tilde{A})$ (8) is minimized with respect to \tilde{A} selecting²

$$\tilde{A} = \hat{A} = \bar{X}(\hat{F}) \tag{15}$$

where $\bar{X}(\hat{F})$ can be computed exactly through its expression (9) or, in an approximate fashion, through a computationally efficient procedure based on the fact that the vector

$$\bar{\mathbf{X}}_{s} \triangleq M \, \mathbf{X}_{0} \tag{16}$$

collects N_0 uniformly spaced samples of the function $\bar{X}(F)$. For this reason, an approximate evaluation of the quantity $\bar{X}(\hat{F})$ at a normalized frequency \hat{F} different from any multiple of F_{DFT} (11) can be accomplished by interpolating the elements of the vector $\bar{\mathbf{X}}_s$ (16); the last vector, in turn, can be easily computed after evaluating the N_0 th FFT of $\mathbf{x}_{0,\text{ZP}}$ (13), i.e., the vector \mathbf{X}_0 (12).

Let us take into consideration now subproblem **P2**. This subproblem, unlike the previous one, does not admit a closed-form solution. For this reason, an approximate solution is developed below. Such a solution is based on representing the normalized frequency F in the same form as \tilde{F} [see (10)], i.e., as $F = F_c + \delta F_{DFT}$ and on a method for estimating the real residual δ , i.e., for accomplishing the *fine estimation* of F. This method is derived as follows. Representing the trial normalized frequency \tilde{F} according to (10) allows us to rewrite the expression (7) (with $\tilde{A} = \hat{A}$) as

$$\varepsilon_n(\tilde{F}, \hat{A}) = |x_n|^2 + |\hat{A}|^2 - 2\Re\{x_n\tilde{A}^* \exp(-j(\hat{\theta}_n + n\tilde{\Delta}))\}$$
(17)

where $\tilde{\Delta} \triangleq 2\pi \tilde{\delta} F_{\text{DFT}}$ and $\hat{\theta}_n \triangleq 2\pi n F_c$. If the normalized frequency F_{DFT} (11) is small enough (i.e., if the FFT order N_0 is large enough), the complex exponential $\exp(-jn\tilde{\Delta})$

²This is a well-known result (see, e.g., [28], Sec. IV]).

appearing in the RHS of the last equation can be approximated as $\exp(-jn\tilde{\Delta}) \simeq 1 - jn\tilde{\Delta} - n^2\tilde{\Delta}^2/2 + jn^3\tilde{\Delta}^3/6$. Then, substitute the RHS of this approximation into that of (17), and then, the resulting expression in the RHS of (5) produces, after some manipulation, the approximate expression

$$\varepsilon_{\text{CSFE}}(\tilde{\Delta}, \hat{A}) \triangleq \varepsilon_{x} + |\hat{A}|^{2} - 2\Re\{\hat{A}^{*}\bar{X}_{0,\rho}\} +$$

$$- 2\tilde{\Delta}\Im\{\hat{A}^{*}\bar{X}_{1,\rho}\} + \tilde{\Delta}^{2}\Re\{\hat{A}^{*}\bar{X}_{2,\rho}\} +$$

$$+ \tilde{\Delta}^{3}\Im\{\hat{A}^{*}\bar{X}_{3,\rho}\}/3$$

$$(18)$$

for the function $\varepsilon(\tilde{F}, \hat{A})$ (5); here

$$\rho \triangleq F_c/F_{\text{DFT}} \tag{19}$$

$$\bar{X}_{k,\rho} \triangleq \frac{1}{N_0} \sum_{n=0}^{N-1} x_{k,n} \exp\left(-j\frac{2\pi n\rho}{N_0}\right)$$
 (20)

for any k and ρ , k = 1, 2, 3 and $x_{k,n} \triangleq n^k \cdot x_n$, with n = 0, 1,..., N - 1. It is important to point out that:

a) if ρ is an integer, the quantity $\bar{X}_{k,\rho}$ (20) represents the ρ th element of the vector

$$\mathbf{X}_{k} = \begin{bmatrix} X_{k,0}, X_{k,1}, \dots, X_{k,N_{0}-1} \end{bmatrix}^{T}$$
 (21)

generated by the N_0 th-order DFT of the zeropadded version $\mathbf{x}_{k,\mathrm{ZP}} = [\mathbf{x}_k^T \mathbf{0}_{(M-1)N}^T]^T$ of the vector $\mathbf{x}_k \triangleq [x_{k,0}, x_{k,1}, \ldots, x_{k,N-1}]^T$;

- b) if ρ is not an integer, the quantity $\bar{X}_{k,\rho}$ can be evaluated exactly on the basis of (20) or, in an approximate fashion, by interpolating I adjacent elements of the N_0 -dimensional vectors \mathbf{X}_k (21), where I denotes the selected interpolation order;
- c) the use of zero padding in the evaluation of the quantity $\bar{X}_{k,\rho}$ improves the interpolation accuracy;
- d) the evaluation of the vectors $\{X_k; k = 1, 2, 3\}$ requires three *additional* FFTs.

Since the function $\varepsilon_{\text{CSFE}}(\tilde{\Delta}, \hat{A})$ (18) is a polynomial of degree 3 in the variable $\tilde{\Delta}$, an estimate $\hat{\Delta}$ of Δ can be obtained by computing the derivative of this function with respect to $\tilde{\Delta}$, setting it to zero and solving the resulting quadratic equation

$$a(\rho)\,\tilde{\Delta}^2 + b(\rho)\,\tilde{\Delta} + c(\rho) = 0 \tag{22}$$

in the variable $\tilde{\Delta}$; here

$$a(\rho) \triangleq \Im\{\hat{A}^* \bar{X}_{3,\rho}\}/2 \tag{23}$$

$$b(\rho) \triangleq \Re{\{\hat{A}^* \bar{X}_{2,\rho}\}} \tag{24}$$

and

$$c(\rho) \triangleq -\Im{\{\hat{A}^* \bar{X}_{1,\rho}\}}.$$
 (25)

Note that only one of the two solutions of (22), namely

$$\hat{\Delta} = -\frac{b(\rho) + \sqrt{(b(\rho))^2 - 4a(\rho)c(\rho)}}{2a(\rho)}$$
 (26)

has to be employed. A simpler estimate of Δ is obtained neglecting the contribution of the first term in the left-hand

side of (22), i.e., setting $a(\rho) = 0$. This leads to a first-degree equation, whose solution is

$$\hat{\Delta} = -c(\rho)/b(\rho). \tag{27}$$

Given an estimate $\hat{\Delta}$ of Δ , the *fine estimate*

$$\hat{F} = F_c + \hat{\Delta}/(2\pi) \tag{28}$$

of F can be evaluated on the basis of (10).

The results derived above allow us to derive an estimation algorithm, called complex single-frequency estimator (CSFE), for iteratively estimating the normalized frequency F and the complex amplitude A. This algorithm is initialized by:

- 1) evaluating:
 - a) the vector \mathbf{X}_0 (12);
 - b) the initial coarse estimate $\hat{F}_c^{(0)}$ of F as

$$\hat{F}_c^{(0)} = \hat{\alpha} F_{\text{DFT}} \tag{29}$$

where the integer $\hat{\alpha}$ is computed by means of the well-known *periodogram method* (e.g., see [28], Sec. IV] or [32], Sec. I]), i.e., as

$$\hat{\alpha} = \arg \max_{\tilde{\alpha} \in \{0, 1, \dots, N_0 - 1\}} \left| \bar{X}_{0, \tilde{\alpha}} \right| \qquad (30)$$

c) the quantity [see (19)]

$$\hat{\rho}^{(0)} \triangleq \hat{F}_c^{(0)} / F_{\text{DFT}} = \hat{\alpha} \tag{31}$$

- d) the initial estimate $\hat{A}^{(0)}$ of A on the basis of (15) with $\hat{F} = \hat{F}_c^{(0)}$;
- e) the spectral coefficients $\bar{X}_{1,\hat{\alpha}}$, $\bar{X}_{2,\hat{\alpha}}$ and $\bar{X}_{3,\hat{\alpha}}$ on the basis of (20);
- f) the coefficients $\{a(\hat{\alpha}), b(\hat{\alpha}), c(\hat{\alpha})\}$ ($\{b(\hat{\alpha}), c(\hat{\alpha})\}$ according to (23)–(25) and the first estimate $\hat{\Delta}^{(0)}$ of Δ on the basis of (26) [or (27)];
- g) the first fine estimate $\hat{F}^{(0)}$ of F on the basis of (28), i.e., as

$$\hat{F}^{(0)} = \hat{F}_c^{(0)} + \hat{\Delta}^{(0)}/(2\pi) \tag{32}$$

2) setting its iteration index i to 1.

Then, an iterative procedure is started. The ith iteration is fed by the estimates $\hat{F}^{(i-1)}$ and $\hat{A}^{(i-1)}$ of F and A, respectively, and produces the new estimates $\hat{F}^{(i)}$ and $\hat{A}^{(i)}$ of the same quantities (with $i=1,2,...,N_{\text{CSFE}}$, where N_{CSFE} is the overall number of iterations); the procedure employed for the evaluation of $\hat{F}^{(i)}$ and $\hat{A}^{(i)}$ consists of the two steps described below (the pth step is denoted CSFE-Sp).

CSFE-S1: The new estimate $\hat{\Delta}^{(i)}$ of Δ is computed through (26) [or (27)]; in the evaluation of the coefficients $\{a(\rho), b(\rho), c(\rho)\}$ ($\{b(\rho), c(\rho)\}$) appearing in the RHS of these equations, $\hat{A} = \hat{A}^{(i-1)}$ and

$$\rho = \hat{\rho}^{(i-1)} \triangleq \hat{F}^{(i-1)} / F_{\text{DFT}} \tag{33}$$

are assumed. Then

$$\hat{F}^{(i)} = \hat{F}^{(i-1)} + \hat{\Delta}^{(i)}/(2\pi) \tag{34}$$

is evaluated.

CSFE-S2: The new estimate $\hat{A}^{(i)}$ of \hat{A} is evaluated through (15); $\hat{F} = \hat{F}^{(i)}$ is assumed in this case. Moreover, the index i is incremented by one before starting the next iteration.

At the end of the last (i.e., of the N_{CSFE} th) iteration, the fine estimates $\hat{F} = \hat{F}^{(N_{\text{CSFE}})}$ and $\hat{A} = \hat{A}^{(N_{\text{CSFE}})}$ of F and A, respectively, become available.

The CSFE is summarized in Algorithm 1. It is important to note the following points.

- 1) The approximate metric $\varepsilon_{\text{CSFE}}(\tilde{\Delta}, \hat{A})$ (18) on which the CSFE is based is new, since it has not been derived in previous work on single-frequency estimation. Note also that none of the known single-frequency estimators relies on the computation of the spectral coefficients $\{X_{k,\rho}; k=1,2,3\}$ employed by the CSFE for the evaluation of the residual δ .
- 2) The estimate $\hat{\delta}^{(i)}$ of δ computed by the CSFE in its *i*th iteration is expected to become smaller as *i* increases, since $\hat{F}^{(i)}$ should progressively approach F if our algorithm converges.
- 3) The estimate $\hat{\Delta}^{(i)}$ evaluated according to (27) is expected to be less accurate than that computed on the basis of (26). However, our numerical results have evidenced that both the solutions achieve similar accuracy. Despite this, (26) is adopted in Algorithm 1 for generality.
- 4) The CSFE can be employed even if the single tone appearing in the RHS of (3) is replaced by the superposition of L distinct tones [see (1)]. In this case, the strongest (i.e., the dominant) tone is usually detected through the periodogram method [see (30)], and the parameters of this tone are estimated in the presence of both Gaussian noise and the interference due to the remaining tones. Therefore, the estimation accuracy of the CSFE is affected by both the amplitudes and the frequencies of the other (L-1) tones.
- 5) If the CSFE algorithm converges, the trend of the sequence $\{\hat{\Delta}^{(i)}; i=1,2,\ldots\}$ is expected to be monotonically decreasing; based on this observation, a simple stopping criterion can be formulated. In fact, the execution of the CSFE can be stopped if, at the end of the ith iteration, the conditions i) $|\hat{\Delta}^{(i)}| < \varepsilon_{\Delta}$ and/or ii) $|\hat{\Delta}^{(i)} \hat{\Delta}^{(i-1)}| < \varepsilon_{\Delta,i}$ are satisfied; here, ε_{Δ} and $\varepsilon_{\Delta,i}$ represent proper thresholds.
- 6) The estimates generated by the CSFE algorithm are *unbiased*, provided that the overall number of iterations it accomplishes is large enough; a proof of this statement is provided in [59], App. D].

B. Estimation of Multiple Tones

Let us analyze now in detail how the techniques derived in the previous paragraph can be exploited to estimate the multiple tones that form the useful component of the complex sequence $\{x_n\}$, when its nth sample is expressed by (1) with L > 1. The recursive method we develop to achieve this target is based on the following basic principles.

Algorithm 1: Complex single frequency estimation

Input: The vectors $\{\mathbf{X}_k; k = 0, 1, 2 \text{ and } 3\}$ [see (21)] and the parameter N_{CSFE} .

1 Initialization:

a- Evaluate X_0 (12) and $\hat{\alpha}$ on the basis of (30); then, compute the initial estimate $\hat{A}^{(0)}$ of A according to (15) and set $\hat{\rho}^{(0)} = \hat{\alpha}[(\text{see (31)}].$ **b-** Evaluate $\bar{X}_{1,\hat{\alpha}}$, $\bar{X}_{2,\hat{\alpha}}$, and $\bar{X}_{3,\hat{\alpha}}$ according to (20); then compute $\{a(\hat{\alpha}), b(\hat{\alpha}), c(\hat{\alpha})\}$ according to (23)–(25). Finally, compute $\hat{\Delta}^{(0)}$ and $\hat{F}^{(0)}$ according to (26) and (28), respectively.

Output: The estimates \hat{F} and \hat{A} of F and A, respectively.

- 1) Tones are *sequentially* detected and estimated.
- 2) The detection of a new tone and the estimation of its parameters are based on the procedure developed for the CSFE in the previous paragraph; in addition, a cancellation algorithm is incorporated in this method to remove the contribution of previously detected tones from all the spectral information [namely, the spectrum $\bar{X}(F)$ (9), the vector \mathbf{X}_0 (12), and the coefficients $\{\bar{X}_{k,\rho}\}$ (20)] that is processed to detect and estimate the new tone.
- 3) After detecting a new tone and estimating its parameters, a *re-estimation technique* is executed to improve the accuracy of both this tone and the previously estimated tones; the proposed technique is inspired by the related methods described in [8], [14], and [15].
- 4) A proper criterion is adopted to stop recursions. This allows us to estimate the (unknown) number of targets, which is the value of the parameter *L*.

The recursive method relying on these principles is called *complex single-frequency estimation and cancellation* (CSFEC). The CSFEC algorithm is initialized by:

1) executing the CSFE, fed by the complex sequence $\{x_n\}$, to generate, through N_{CSFE} iterations, the initial estimates $\hat{F}_0[0]$ and $\hat{A}_0[0]$ of the normalized frequency and the complex amplitude, respectively, of the first detected tone:

2) setting the recursion index r to 1.

Then, a recursive procedure is started. The *r*th recursion is fed by the vectors

$$\mathbf{\hat{F}}[r-1] = \left[\hat{F}_0[r-1], \hat{F}_1[r-1], \dots, \hat{F}_{r-1}[r-1]\right]^T$$
 (35)

and

$$\hat{\mathbf{A}}[r-1] = \left[\hat{A}_0[r-1], \hat{A}_1[r-1], \dots, \hat{A}_{r-1}[r-1]\right]^T$$
(36)

collecting the frequencies and the associated complex amplitudes characterizing the r tones detected and estimated in the previous (r-1) recursions and generates the new vectors

$$\hat{\mathbf{F}}[r] = \left[\hat{F}_0[r], \hat{F}_1[r], \dots, \hat{F}_r[r]\right]^T$$
 (37)

and

$$\hat{\mathbf{A}}[r] = [\hat{A}_0[r], \hat{A}_1[r], \dots, \hat{A}_r[r]]^T$$
 (38)

after:

- a) estimating the frequency $\hat{F}_r[r]$ and the associated complex amplitude $\hat{A}_r[r]$ of a new (i.e., of the *r*-th) tone (if any);
- b) *refining* the estimates of the *r* tones available at the beginning of the considered recursion. The procedure employed for accomplishing all this consists of the three steps described below (the *p*th step is denoted CSFEC-S*p*).

CSFEC-S1 (CSFE initialization with cancellation): In this step, the following quantities are evaluated (see the *initialization* part of Algorithm 1).

1) The residual spectrum

$$\mathbf{X}_{0}[r] = \left[X_{0,0}[r], X_{0,1}[r], \dots, X_{0,N_{0}-1}[r] \right]^{T}$$

$$\triangleq \mathbf{X}_{0} - \mathbf{C}_{0}(\mathbf{\hat{A}}[r-1], \mathbf{\hat{F}}[r-1], r)$$
(39)

where \mathbf{X}_0 is the N_0 th-order DFT of the zero-padded version $\mathbf{x}_{0,\mathrm{ZP}}$ of the vector \mathbf{x}_0 collecting all the elements of the sequence $\{x_n\}$ [see (13) and (14)] and the N_0 -dimensional vector

$$\mathbf{C}_{0}(\hat{\mathbf{A}}[r-1], \hat{\mathbf{F}}[r-1], r)$$

$$\triangleq \sum_{l=0}^{r-1} \bar{\mathbf{C}}_{0}(\hat{A}_{l}[r-1], \hat{F}_{l}[r-1])$$
(40)

represents the contribution given by all the estimated tones to \mathbf{X}_0 (in particular, $\bar{\mathbf{C}}_0(\hat{A}_l[r-1],\hat{F}_l[r-1])$ is the contribution provided by the lth tone to the vector \mathbf{X}_0 (the expression of this vector can be found in the Appendixes). If the overall energy $\mathcal{E}_0[r] \triangleq |\mathbf{X}_0[r]|^2$ satisfies the inequality $\mathcal{E}_0[r] < \mathcal{T}_{\text{CSFEC}}$, where $\mathcal{T}_{\text{CSFEC}}$ is a proper threshold, the algorithm stops and the estimate $\hat{L} = r$ of L is generated.

2) The integer [see (30)]

$$\hat{\alpha}[r] = \arg \max_{\tilde{\alpha} \in \{0, 1, \dots, N_0 - 1\}} |X_{0, \tilde{\alpha}}[r]|$$
 (41)

that represents the index of the element of $\mathbf{X}_0[r]$ (39) having the largest absolute value.

3) The preliminary estimate [see (15)]

$$\bar{A}_r[r] = \bar{X}(\hat{F}_{c,r}[r]) - \bar{X}_{lk,0}(\hat{\mathbf{A}}[r-1], \hat{\mathbf{F}}[r-1], \hat{F}_{c,r}[r])$$
(42)

of the complex amplitude of the new tone; here, $\hat{F}_{c,r}[r] = \hat{\alpha}[r] F_{\text{DFT}}$ and

$$\bar{X}_{lk,0}(\hat{\mathbf{A}}[r-1], \hat{\mathbf{F}}[r-1], \hat{F}_{c,r}[r])
\triangleq \sum_{l=0}^{r-1} \bar{X}_0(\hat{A}_l[r-1], \hat{F}_l[r-1], \hat{F}_{c,r}[r])$$
(43)

represent the *coarse estimate* of the frequency of the new tone [see (29)], and the contribution given to $\bar{X}(F)$ by all the estimated tones (i.e., the *leakage*) at the frequency $F = \hat{F}_{c,r}[r]$ (in particular, $\bar{X}_0(\hat{A}_l[r-1], \hat{F}_l[r-1], \hat{F}_{c,r}[r])$ is the leakage due to the *l*th tone; the expression of the function $\bar{X}_{lk,k}(\hat{A}, \hat{F}, \bar{F})$ is provided in the Appendixes).

4) The spectral coefficient

$$\bar{X}_{k,\rho[r]}[r] = \bar{X}_{k,\rho[r]} - \hat{X}_{lk,k} (\hat{\mathbf{A}}[r-1], \hat{\mathbf{F}}[r-1], \hat{F}_{c,r}[r])$$
(44)

for k=1,2 and 3; here, we have that [see (31)] $\rho[r] = \hat{F}_{c,r}[r]/F_{\rm DFT} = \hat{\alpha}[r]$ and

$$\hat{X}_{lk,k}(\hat{\mathbf{A}}[r-1], \hat{\mathbf{F}}[r-1], \hat{F}_{c,r}[r])$$

$$\triangleq \sum_{l=1}^{r-1} \bar{X}_{lk,k}(\hat{A}_{l}[r-1], \hat{F}_{l}[r-1], \hat{F}_{c,r}[r]) \quad (45)$$

is the contribution given to $\bar{X}_{k,\rho[r]}[r]$ by all the estimated tones (i.e., the *leakage*) at the frequency $\hat{F}_{c,r}[r]$ (in particular, $\bar{X}_{lk,k}(\hat{A}_l[r-1],\hat{F}_l[r-1],\hat{F}_{c,r}[r])$ represents the leakage due to the *l*th estimated tone).

5) The coefficients $a(\hat{\alpha}[r])$, $b(\hat{\alpha}[r])$, and $c(\hat{\alpha}[r])$, the residual $\hat{\Delta}^{(0)}[r]$, and the normalized frequency

$$\hat{F}_r^{(0)} = \hat{F}_{c,r}[r] + \hat{\Delta}^{(0)}[r]/(2\pi) \tag{46}$$

on the basis of (23)–(25), (26) [or (27)], (29), and (32). Note that $\hat{F}_r^{(0)}$ represents the *initial fine estimate* of the normalized frequency of the new tone.

The evaluation of the frequency $\hat{F}_r^{(0)}$ (46) concludes the initialization of the modified CSFE executed for the detection and the estimation of the new tone.

CSFEC-S2 (CSFE refinement with cancellation): After carrying out the first step, N_{CSFE} iterations³ are executed to refine the estimate of the parameters of the new tone. The processing accomplished in this step follows closely that described in the *refinement* part of Algorithm 1. For this reason, in each iteration, a new estimate of the complex amplitude and of the residual of frequency of the *r*th tone are computed. This requires reusing (42)–(44) in order to remove the leakage in the spectrum $\bar{X}(F)$ and in the coefficients $\bar{X}_{k,\rho}$ (see steps $\bf c$ and $\bf d$, respectively, of Algorithm 1).

³The potential dependence of the parameter N_{CSFE} on the recursion index r is ignored here for simplicity.

At the end of the last iteration, the frequency $\hat{F}_{\text{CSFE},r}[r]$ and the associated complex amplitude $\hat{A}_{\text{CSFE},r}[r]$ of the new tone are available; these represent $\hat{F}_r[r]$ and $\hat{A}_r[r]$, respectively, if the following re-estimation step is not accomplished.

CSFEC-S3 (re-estimation): This step is fed by the (r+1) normalized frequencies $\{\hat{F}_0[r-1], \hat{F}_1[r-1],$..., $\hat{F}_{r-1}[r-1]$, $\hat{F}_{CSFE,r}[r]$ and the associated complex amplitudes $\{\hat{A}_0[r-1], \hat{A}_1[r-1], ..., \hat{A}_{r-1}[r-1], \hat{A}_{CSFE,r}[r]\}.$ It consists in repeating the previous step for each of the detected tones, starting from the first tone and ending with the (r+1)th one. This means that, when re-estimating the *l*th tone, the leakage due to the tones whose index belongs to set $\{0, 1, \dots, l-1, l+1, \dots, r\}$ has to be removed by exploiting equations similar to (42), (44), and (45), with l = 0, 1, ..., r. This allows us to progressively refine the amplitude and the frequency of each tone, so generating the final frequencies $\{\hat{F}_0[r], \hat{F}_1[r], ..., \hat{F}_r[r]\}$ and their complex amplitudes $\{\hat{A}_0[r], \hat{A}_1[r], ..., \hat{A}_r[r]\}$. Note that, in principle, the re-estimation can be accomplished multiple (say, N_{RES}) times.

Our simulation results have evidenced that, unluckily, the estimates generated by the CSFEC algorithm are biased if the values selected for the parameters N_{CSFE} and N_{RES} are not large enough.⁴ In principle, this bias can be arbitrarily reduced by increasing the values of these parameters. However, we found out that a computationally efficient alternative to this approach is represented by running an additional (i.e., a fourth) step once that the CSFEC algorithm has been executed. In this final step, the estimation algorithm developed by Ye and Aboutanios [40], [41] is carried out after initializing it with the estimates $\{\hat{F}_0[\hat{L}], \hat{F}_1[\hat{L}], ...,$ $\hat{F}_{\hat{l}-1}[\hat{L}]$ and their complex amplitudes $\{\hat{A}_0[\hat{L}], \hat{A}_1[\hat{L}], \dots, \hat{A}_n[\hat{L}]\}$ $\hat{A}_{\hat{l}-1}[\hat{L}]$ generated by the CSFEC. The hybrid technique resulting from interconnecting the CSFEC algorithm with the above-mentioned algorithm is dubbed hybrid CSFEC (HCSFEC). Finally, the following points are worth noting.

- 1) The oversampling factor M adopted in the computation of the vectors $\{\mathbf{X}_k^{(l)}\}$ and the stopping criterion employed by the CSFE need to be carefully adjusted in order to achieve a good accuracy in the estimation of the parameters of each new tone.
- 2) The poor estimation of the normalized frequency F_l and/or of the complex amplitude A_l may lead to significant *error accumulation* if CSFEC-S3 is removed; readers should also keep in mind that a fundamental role in accurate cancellation is played by the accuracy of the estimated frequency residual.
- 3) The threshold $\mathcal{T}_{\text{CSFEC}}$ needs to be properly adjusted in order to ensure that the probability that \hat{L} is equal to L is close to unity. On the one hand, a large value of $\mathcal{T}_{\text{CSFEC}}$ may lead to miss weaker tones; on the other hand, a small value of this parameter may lead to the identification of nonexistent tones.

C. Comparison With Other Estimation Methods

The CSFEC technique developed in Sections III-A and III-B is conceptually related to the *multiple-tone estimators* developed by Gough [14], Li and Stoica [15], Macleod [8], Ye and Aboutanios [40], [41], Serbes and Qaraqe [42], Serbes [43], and Djukanović and Popović-Bugarin [44] (these algorithms are denoted CLEAN, RELAX, Alg-M, Alg-YA, CFH, Alg-S, and Alg-DP, respectively, in the following). In fact, all these algorithms are recursive and rely on a serial cancellation procedure, since, within each recursion, they detect a single tone, estimate its parameters, and subtract its contribution from the residual signal emerging from the previous iteration. Despite their similar structures, they exhibit various differences that concern the three specific issues listed below.

- 1) Single-frequency estimator: The main difference is represented by the method they employ in the estimation of a single tone. On the one hand, the CLEAN and RELAX algorithms rely on the coarse estimate generated by the periodogram method for each detected tone and, eventually, exploit zero padding to improve spectral resolution. On the other hand, the Alg-M, the Alg-DP, the Alg-YA, the Alg-S, and the CFH algorithm compute the frequency residual by means of open-loop interpolation or iterative methods; the last methods refine the estimate of the frequency residual through multiple iterations. All the single-tone estimators employed in these algorithms differ from the one used in CSFEC and HCSFEC.
- 2) Use of a re-estimation procedure: In the CLEAN and RELAX algorithms and in Alg-M, once a new tone has been estimated, all the previously computed tones are re-estimated by subtracting the contribution of all the other tones; tone cancellation is accomplished in the time domain in the CLEAN and RELAX algorithms, whereas it is carried out in the frequency domain in the Alg-M. The last approach is also adopted in our estimation algorithms. Finally, the CFH algorithm, the Alg-S, the Alg-YA, and the Alg-DP accomplish re-estimation after computing a coarse estimate of all the parameters of the detected tones. However, the Alg-DP and the CFH algorithm execute this task only once, whereas the Alg-S and the Alg-YA repeat it a given number of times.
- 3) *Use of oversampling:* In the technical literature, the use of oversampling has been proposed for the CLEAN, the RELAX, the Alg-S, and the CSFEC and HCSFEC algorithms only.

D. Computational Complexity

The complexity of the estimation algorithm developed in Section III-A has been carefully assessed in terms of the number of floating point operations to be executed in the detection of L targets. The general criteria adopted in estimating the overall computational cost of the CSFE algorithm are summarized in [59], App. C], where a detailed

 $^{^{4}}$ In our simulation results, the values $N_{\rm CSFE} = 15$ and $N_{\rm RES} = 5$ have been selected. However, such parameters can take on different values depending on the SNR; for instance, $N_{\rm RES}$ can be increased if the SNR is poor.

TABLE I
Order of the Computational Complexity of Various Estimation Algorithms

Algorithm	CLEAN / RELAX	Alg-M	Alg-YA / Alg-S	CFH / Alg-DP
$\mathcal{O}(\cdot)$	$L^2N_0\log_2(N_0)$	$N_0 \log_2(N_0) + L^2 K_M$	$LN \log_2(N) + LQN$	$LN \log_2(N)$

analysis of the contributions due to the different tasks accomplished by each of them is also provided. Our analysis leads to the conclusion that this cost is approximately of order $\mathcal{O}(M_{\text{CSFE}})$, with

$$M_{\text{CSFE}} = N_0 \log_2 N_0 + K_{\text{CSFE}} N_{\text{CSFE}} I^2.$$
 (47)

Here, $N_{\rm CSFE}$ represents the overall number of iterations accomplished by the CSFE and $K_{\rm CSFE}=1/2$. Our computer simulations have evidenced that, in the scenarios we considered, a small value of I is required if the so-called barycentric interpolation is employed (see [60]). For this reason, the contribution of the second term appearing in the RHS of (47) can be neglected, so that the order of the overall computational cost is well approximated by the first term, i.e., from the term that originates from FFT processing. Moreover, based on the last result, it is not difficult to show that the computational cost of the CSFEC algorithm is approximately of order $\mathcal{O}(M_{\rm CSFEC})$, with

$$M_{\text{CSFEC}} = N_0 \log_2(N_0) + K_{\text{CSFE}} L N_{\text{CSFE}} I^2 \qquad (48)$$

if no re-estimation is accomplished (see CSFEC-S3 in the description of the CSFEC algorithm), and the algorithm stops after detecting the last tone. Note that the first term appearing in the RHS of (48) accounts for the initialization [and, in particular, for the computation of the vectors \mathbf{X}_0 (12) and $\{X_k\}$ (21)], whereas the second term accounts for the fact that, in the CSFEC algorithm, the CSFE is executed L times. It is also worth pointing out that the computational costs due to the evaluation of the estimated tones detected after the first one and to their frequency-domain cancellation do not play an important role in this case. However, if re-estimation is accomplished, the parameter L appearing in the RHS of (48) is replaced by L^2 , since this task involves all the estimated tones. Despite this, the increase in the overall computational cost of the CSFEC with respect to the CSFE is limited since, as evidenced by our simulation results, the use of re-estimation allows these algorithms to achieve convergence with a smaller value of the parameter $N_{\rm CSFE}$.

Finally, it is important to compare the computational cost of the CSFEC algorithm with that of the CLEAN, RELAX, Alg-M, Alg-YA, CFH, Alg-S, and Alg-DP techniques considered in the previous paragraph. Their order of complexity is listed in Table I (where K_M represents the computational cost of single-tone estimation), from which the following considerations can be easily inferred.

1) The CLEAN and RELAX algorithms are characterized by the same order, expressed by the complexity of a zero-padded FFT multiplied by L^2 ; the last factor

- is due to the fact that tone re-estimation is employed in both the algorithms.
- 2) The Alg-M is characterized by the lowest computational cost; in fact, since it performs the cancellation of the detected tones directly in the frequency domain, tone estimation does not require the computation of additional FFTs. Moreover, since tone re-estimation is employed, the cost for the estimation of a single tone (i.e., the parameter K_M appearing in Table I) is multiplied by L^2 .
- 3) The order of complexity of the Alg-YA, the Alg-S, the Alg-DP, and the CFH algorithm depends on the fact that one FFT is computed for the estimation of each tone; moreover, an additional term equal to LQN is included in the order of the Alg-YA and the Alg-S, since these estimate all the tones Q times.
- 4) The order of the cost of the CSFEC algorithm is similar to that of the Alg-M; however, in this case, three (or four) FFTs are computed in the initialization phase and the cost for the estimation of each tone is multiplied by N_{CSFE}, since tone refinement is performed within each recursion.

IV. NUMERICAL RESULTS

In this section, the accuracy and robustness of the proposed algorithms is assessed on the basis of both synthetically generated data and experimental data acquired through an FMCW colocated MIMO radar.

A. Numerical Results Based on Synthetically Generated Measurements

In this section, we compare, in terms of accuracy, convergence rate, and failure probability, our single-frequency estimator (CSFE) with the A&M [32], the QSE and HAQSE algorithms [48], and the CSFEC and HCSFEC algorithms with the CFH algorithm [42], the Alg-YA [40], [41], the Alg-S [43], and the Alg-DP [44]. As far as the A&M algorithm is concerned, two versions of it are considered; such versions are denoted A&M#1 and A&M#2 in the following and correspond to Alg-1 and Alg-2, respectively, described in [32].

Five different scenarios have been considered in our computer simulations. In all of them, N = 512 and $f_s = N$ Hz have been selected for the overall number of samples of the sequence $\{x_n\}$ and the sampling frequency, respectively; moreover, for any L, the phases of the L overlapped tones have been randomly selected over the interval $[0, 2\pi]$, each independently of all the other ones. The specific features of the simulated scenarios can be summarized as follows.

Scenario #1 (S1): This is characterized by L=1, i.e., by a single tone, having amplitude equal to 1 and whose normalized frequency is uniformly distributed over the interval [8/N, 28/N].

Scenario #2 (S2): This is characterized by L=2, i.e., by a couple of tones, both having amplitude equal to 1. Moreover, the normalized frequency F_0 of the first tone is uniformly distributed over the interval [8/N, 28/N], whereas that of the second one is $F_1 = F_0 + 1.1/N$.

Scenario #3 (S3): This is characterized by L=2, i.e., by a couple of tones, both having amplitude equal to 1. Moreover, the normalized frequency F_0 of the first tone is uniformly distributed over the interval [8/N, 28/N], whereas that of the second one is $F_1 = F_0 + \Delta F_d$; here, $\Delta F_d \triangleq (1 + 0.05 \, d)/N$ represents the normalized frequency spacing between the two tones and is controlled through the nonnegative parameter d (d=0,1,...,10 is assumed in the following).

Scenario #4 (S4): This is characterized by $L \in \{2, 3, ..., 10\}$, i.e., by a varying number of tones. For any L, the amplitude and the frequency of the kth tone are given by

$$a_k \triangleq 10^{-k \, \Delta_a/10} \tag{49}$$

and $F_k \triangleq F_0 + 1.8 \, k/N$, respectively, with k = 0, 1, ..., L - 1; here, $\Delta_a = 2.5/3$ and F_0 is uniformly distributed over the interval [8/N, 28/N].

Scenario #5 (S5): This is characterized by L=10 tones, whose amplitudes follow the law expressed by (49). Moreover, the normalized frequency of the kth tone is $F_{k,m} \triangleq F_0 + k \Delta F_m$, with $F_0 = 8.3/N$ and k = 0, 1,..., 9; here, $\Delta F_m = (1.5 + 0.2 \, m)/N$ represents the normalized frequency spacing between adjacent tones and is controlled through the nonnegative parameter m (m = 0, 1,..., 5 is assumed in the following).

It is important to note the following points.

- 1) The interest in **S1** has been uniquely motivated by the need of comparing the performance of the CSFE with that achieved by the other single-frequency estimators.
- 2) The study of **S2** and **S3** has allowed us to assess how the considered multiple-tone estimators perform in the presence of two close tones whose spacing is fixed and variable, respectively, whereas that of **S4** how their performance changes when *L* increases.
- 3) The fifth scenario refers to the case in which the observed signal contains many closely spaced tones

- having different strengths, so that multiple-tone estimators may fail detecting all of them and/or the quality of the estimates of their parameters may be quite poor.
- 4) In **S1–S3**, the normalized frequency F_0 of the first tone has been randomly generated to average out the influence of the frequency residual on estimation accuracy.

In our computer simulations, the following performance indices have been assessed for each of the analyzed algorithms:

- 1) the probability of failure (P_f) , i.e., the probability that the considered algorithm does not converge. In our simulation, a failure event is detected whenever the absolute value of the normalized frequency error characterizing the final frequency estimate exceeds the threshold $\Delta \varepsilon_F \triangleq 1/(2N_0)$, i.e. it is greater than half the size of the frequency bin characterizing FFT processing;
- 2) the *root-mean-square error* (RMSE) for the estimate of the normalized frequency (denoted RMSE $_f$). Note that, whenever frequency estimation is efficient, amplitude and phase estimation are also efficient; for this reason, the RMSE of amplitude and phase is not provided.

It is important to stress that limited attention to the first parameter has been paid in the technical literature and that its value depends on the intensity of both the additive noise and the interference experienced by each newly detected tone (and due to uncanceled tones). Our interest in it can be motivated as follows. Each of the considered frequency estimation algorithms is highly nonlinear; for this reason, its behavior is characterized by a threshold, whose value depends on the specific scenario in which it is employed. In practice, if a frequency estimation algorithm operates above its threshold, failures are very rare events; consequently, the assessed RMSEs are negligibly influenced by them, i.e., they account for the intensity of the errors observed after the convergence of the algorithm itself. On the contrary, if the algorithm operates below its threshold, a portion of its estimation errors (but not all of them) refers to situations in which it has not converged; when this happens, large frequency estimation errors (i.e., outliers) may be observed. In the last case, RMSEs are not so meaningful since they account for two heterogeneous contributions. It is also worth mentioning that a failure event does not necessarily occurs in the case of a wrong selection of the frequency bin in the coarse estimation stage [see (30)]; in fact, in some cases, frequency estimation algorithms do not exhibit failures (i.e., frequency outliers) even if the output of their coarse estimation step is wrong. The significance of these considerations and our interest in the probability of failure can be fully appreciated by analyzing the simulation results shown in Fig. 1(a) and (b) that refer to the A&M#1 algorithm operating in S1. In particular, the dependence of $RMSE_f$ and P_f on the SNR for this algorithm is illustrated

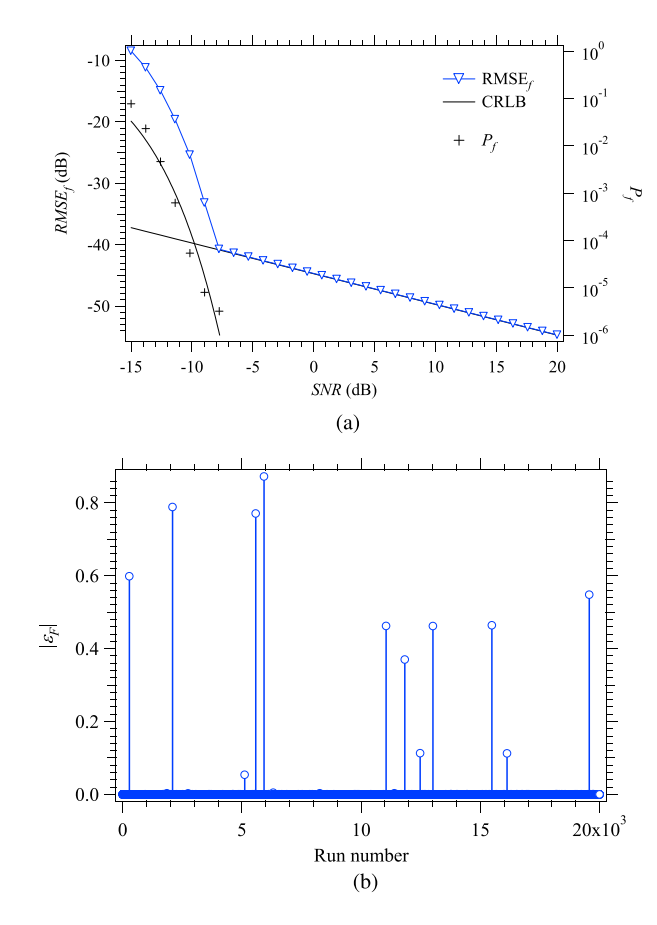


Fig. 1. Some numerical results referring to the A&M#1 algorithm (first scenario). (a) RMSE performance versus SNR; the CRLB is also shown for comparison. (b) Normalized frequency error versus run number.

in Fig. 1(a) (where the Cramer-Rao lower bound (CRLB) is also shown for comparison), whereas a sample of the absolute value of the normalized frequency errors observed over 20 000 consecutive runs at an SNR = -10 dB is represented in Fig. 1(b); in this case, the overall number of iterations $N_{\text{A\&M}} = 2$ has been adopted for the considered algorithm and 10⁷ simulation runs have been executed to generate the numerical results appearing in the first figure. As can be easily inferred from Fig. 1(a), the A&M#1 algorithm attains the CRLB above its threshold, which, in S1, is found at an SNR \cong -8 dB and corresponds to a P_f approximately equal to 10^{-6} ; below this SNR (that, in the case of a single tone, uniquely identifies the threshold of the algorithm), the estimated RMSE $_f$ is significantly influenced by the presence of outliers, some of which are clearly visible in Fig. 1(b). Other numerical results, not included in this article for space limitations, have also evidenced that the SNR threshold characterizing each algorithm can be identified in correspondence to a P_f approximately equal to 10^{-6} for any value of N. This is equivalent to identifying the SNR threshold, above which the probability of having an outlier is very small. Our simulations have also evidenced that, if all the failure events are ignored in the evaluation of the RMSEs, the (negligible) gap between the RMSE $_f$ of the A&M#1 and the CRLB does not change if the SNR drops

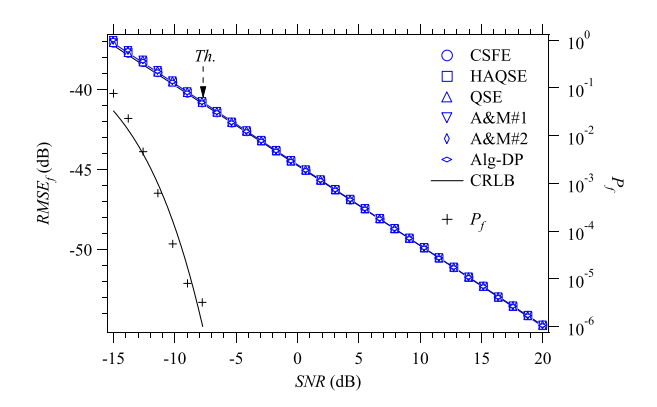


Fig. 2. RMSE performance achieved in frequency estimation versus SNR (first scenario). The Alg-DP and the CSFE, HAQSE, QSE, A&M#1, and A&M#2 algorithms are considered. The CRLB is also shown for comparison.

below its threshold. Based on these considerations, we have decided to:

- assess the probability of failure in all the considered scenarios;
- ignore the failure events in the evaluation of all the RMSEs.

On the one hand, the first choice has allowed us to assess, in all the mentioned scenarios, if each of the considered estimation algorithms is operating above its threshold or below it; in doing so, we have assumed that the threshold is conventionally identified by $P_f = 10^{-6}$, i.e., by one failure over 10^6 runs on the average. On the other hand, the second choice has been made to verify if its accuracy is close to the CRLB when its failures are ignored. In the following, various simulation results are illustrated for the five scenarios described above; in all the cases, each value of the considered performance indices has been evaluated by executing 10^6 runs.

The performance of six single-tone estimators, namely, the Alg-DP, the CSFE, and the A&M#1, A&M#2, QSE, and HAQSE algorithms, has been assessed in S1. The following parameters have been selected for them: 1) the overall number of iterations $N_{\text{CSFE}} = 25$ and interpolation order⁵ I = 7 for the CSFE; 2) the overall number of iterations $N_{\text{A\&M}} = 2$ for the two A&M algorithms; 3) $N_{\text{OSE}} = 3$ for the QSE algorithm; 4) $N_{\text{HAQSE}} = 2$ for the HAQSE algorithm; and 5) frequency displacement $f_d = 1/(10N)$ for the Alg-DP. In addition, the parameter q of the QSE and HAQSE algorithms has been evaluated on the basis of [48], (39)], and the oversampling factor M = 1 has been selected for all the considered algorithms. Some numerical results referring to S1 are illustrated in Fig. 2 (in this figure and in all the following ones, numerical results are represented by markers, whereas lines are drawn to ease reading; moreover,

⁵In all our simulations, the *barycentric interpolation* described in [60] has been always employed. Moreover, the value of $N_{\rm CSFE}$ has been selected based on the simulation results obtained in a worst-case scenario (i.e., characterized by a normalized frequency residual $\delta = 0.5$).

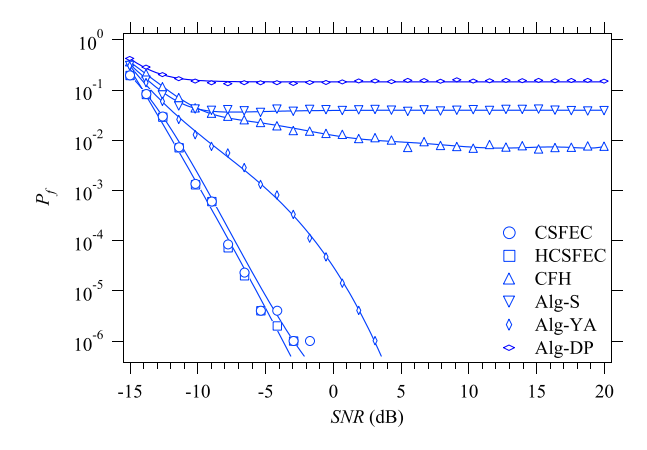


Fig. 3. Probability of failure versus SNR (second scenario). The Alg-S, the Alg-YA, the Alg-DP, and the CSFEC, HCSFEC, and CFH algorithms are considered.

the abbreviation "Th." is employed for the *threshold*, whose position is always indicated by a black arrow). More specifically, the dependence of $RMSE_f$ on the SNR is represented in Fig. 2 for all the considered algorithms. In this figure, the dependence of the probability of failure on the SNR (which is approximately the same for all the considered algorithms) is also shown (the SNR range [-15, 20] dB is considered). From these results, it is easily inferred that: 1) all the considered algorithms exhibit a similar dependence of $RMSE_f$ on

$$SNR \triangleq 1/\sigma^2 \tag{50}$$

and their accuracy approaches the CRLB [61] for SNR∈ [-8, 20] dB; 2) they are characterized by a similar probability of failure and, therefore, by a similar SNR threshold; and 3) they attain the CRLB even below their threshold if failure events are ignored. Our simulation results have also evidenced that the CSFE is characterized by a lower convergence rate than the other algorithms. As far as the last point is concerned, it is worth mentioning that: 1) the A&M#1, A&M#2, QSE, and HAQSE algorithms usually require two to four iterations to achieve convergence, whereas the overall number of iterations required by the CSFE is three to four times larger; 2) the Alg-DP, A&M#1, A&M#2, QSE, and HAQSE algorithms are characterized by similar computation times (CTs), whereas the CSFE is about ten times slower. For this reason, the adoption of the CSFE in single-tone estimation is not recommended. Further numerical results, not shown here for space limitations and referring to an SNR = 10 dB, have shown that the $RMSE_f$ of all the considered estimators exhibit a similar dependence on N, when this parameter ranges from 16 to 2048; moreover, in all the cases, their accuracy approaches the CRLB.

Some numerical results referring to S2 are illustrated in Figs. 3 and 4. More specifically, the dependence of P_f on the SNR is illustrated in Fig. 3, whereas the

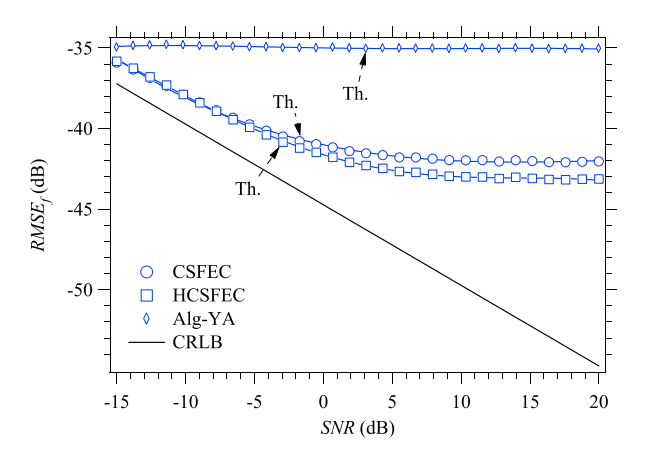


Fig. 4. RMSE performance achieved in frequency estimation versus SNR (second scenario). The Alg-YA and the CSFEC and HCSFEC algorithms are considered. The CRLB is also shown for comparison.

dependence of RMSE $_f$ on the SNR 6 is represented in Fig. 4, for all the considered algorithms; once again, the SNR range [-15, 20] dB is considered. The accuracy of six multiple-tone estimators, namely, the Alg-YA, the Alg-S, the Alg-DP, and the CSFEC, HCSFEC, and CFH algorithms, has been assessed in this case; moreover, the following parameters have been selected for these algorithms in S2 and in the remaining three scenarios: 1) overall number of iterations $N_{\text{CSFE}} = 15$, number of re-estimations $N_{\rm RES} = 5$, and interpolation order I = 7 for the CSFEC;⁷ 2) $N_{\text{CSFE}} = 5$, $N_{\text{RES}} = 1$, I = 7, and number of Alg-YA iterations $N_{YA} = 5$ for the HCSFEC algorithm; 3) the same parameters as the HAQSE and Alg-DP in S1 for the CFH algorithm and the Alg-DP, respectively; and 4) an overall number of iterations Q = 2 for the Alg-YA. Moreover, the number of re-estimations carried out by the Alg-S has been evaluated on the basis of [43], (33)]. Our results show that: 1) the CSFEC and HCSFEC techniques are more robust than all the other estimators, since they achieve a substantially lower probability of failure for an SNR > -10 dB; 2) the thresholds of the CSFEC and HCSFEC algorithms are about -3 dB and are substantially lower than that of Alg-YA, which is found at about 3 dB; 3) the CFH, the Alg-S, and the Alg-DP exhibit a $P_f > 10^{-2}$ for all the values of SNR (therefore, their RMSE performance is ignored in the following); 4) the Alg-YA is always outperformed by the CSFEC and HCSFEC algorithms; 5) the trend in the accuracy of the CSFEC and HCSFEC algorithms diverges from that of the CRLB for an SNR > -6 dB because of the small bias introduced by the serial cancellation procedure on which they are based; 6) the CSFEC algorithm is slightly outperformed by the HCSFEC algorithm for an SNR > -6dB; and 7) the trend in the accuracy of the Alg-YA below its threshold diverges from that of the CRLB for all the SNR values, whereas that of the CSFEC and HCSFEC algorithms

 $[\]overline{^6}$ Since the amplitudes of both the tones are equal to 1, the SNR is still computed on the basis of (50).

⁷The values of the parameters $N_{\rm CSFE}$ and $N_{\rm RES}$ have been selected based on our simulation results obtained for a tone spacing equal to 1.1/N.

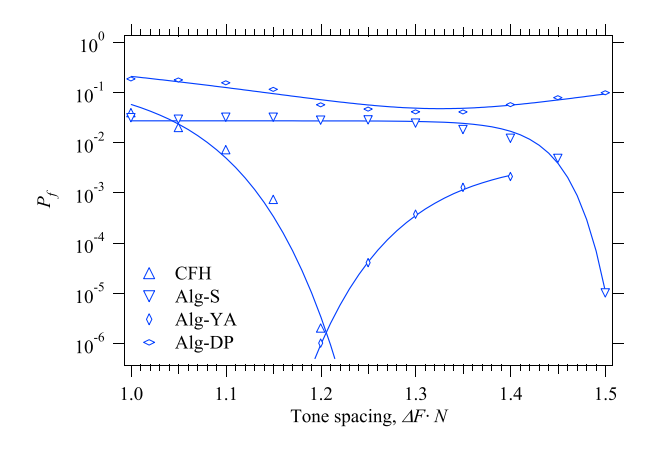


Fig. 5. Probability of failure versus normalized tone spacing (third scenario). The Alg-S, the Alg-YA, the Alg-DP, and the CSFEC, HCSFEC, and CFH algorithms are considered.

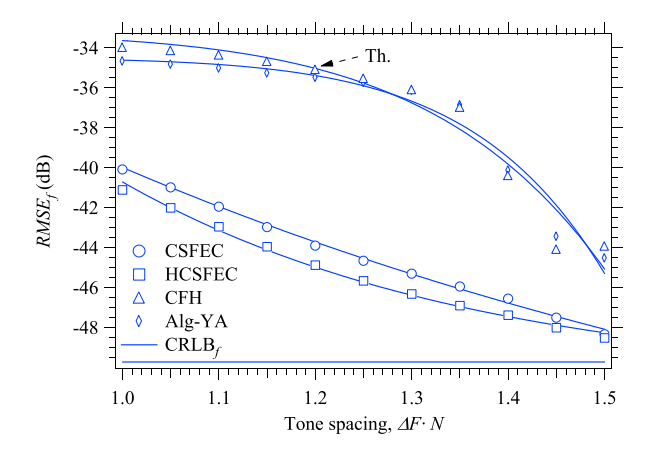


Fig. 6. RMSE performance achieved in frequency estimation versus tone separation (third scenario). The Alg-YA, and the CSFEC, HCSFEC, and CFH algorithms are considered. The CRLB is also shown for comparison.

is only 1 dB far from the corresponding CRLB. The ability of the CSFEC algorithm, the HCSFEC algorithm, and the Alg-YA to estimate correctly both tones is due to their use of a leakage cancellation step. It is also worth mentioning that the CFH algorithm, the Alg-YA, and the Alg-DP require similar CTs, whereas the HCSFEC algorithm and the Alg-S (the CSFEC algorithm) are about two (16) times slower. Additional computer simulations have been run at an SNR = 10 dB in order to assess the dependence of both RMSE_f and P_f on N for all the considered estimators. Our numerical results, not shown here for space limitations and referring to $N = 2^b$ (with b = 4, 5, ..., 11), have evidenced that: 1) the CFH algorithm, the Alg-S, and the Alg-DP always exhibit a $P_f > 10^{-2}$; 2) the CSFEC and HCSFEC algorithms (the Alg-YA) are characterized by a $P_f < 10^{-6}$ for N > 32 (N > 64); and 3) the CSFEC and HCSFEC algorithms are always more accurate than the Alg-YA. Let us focus now on S3. In this scenario, all the performance indices have been evaluated for different values of the normalized tone spacing ($\Delta F \cdot N$). Some numerical results referring to this scenario are illustrated in Figs. 5 and 6. More specifically, the dependence of P_f on the tone spacing

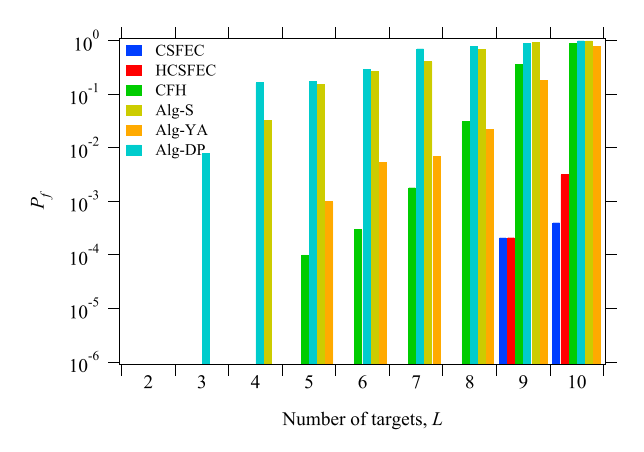


Fig. 7. Probability of failure versus overall number of tones (fourth scenario). The Alg-S, the Alg-YA, the Alg-DP, and the CSFEC, HCSFEC, and CFH algorithms are considered.

is illustrated in Fig. 5, whereas the dependence of RMSE $_f$ on the tone spacing is represented in Fig. 6, for all the considered algorithms; an SNR = 10 dB is assumed. From our results, it can be inferred that: 1) the CSFEC and HCSFEC algorithms are substantially more robust than all the other estimators, since no failure event has been detected for the considered tone spacings over all the simulation runs; 2) the CFH algorithm exhibits a $P_f < 10^{-6}$ for a tone spacing greater than 1.2, whereas the Alg-YA exhibits a $P_f > 10^{-6}$ for values of tone spacing between 1.2 and 1.4; 3) the Alg-S and the Alg-DP are characterized by a $P_f > 10^{-6}$ for any value of tone spacing (for this reason, they are ignored in the following); 5) the Alg-YA and the CFH algorithm are outperformed by the CSFEC and HCSFEC algorithms, for all the considered tone spacings; 6) the CSFEC algorithm is slightly outperformed by the HCSFEC algorithm; and 7) the CSFEC and HCSFEC algorithms attain the CRLB for a tone spacing equal to 1.5.

As already mentioned above, our simulations for S4 have allowed us to assess how the performance of the considered algorithms is influenced by the overall number of tones. Some results referring to this scenario are shown in Fig. 7, which shows the dependence of P_f on L; M = 1 and an $SNR = 10 \, dB$ for the strongest tone have been assumed. From this figure, it is easily inferred that: 1) the Alg-DP (Alg-S) exhibits a $P_f > 10^{-2}$ for $L \ge 3$ ($L \ge 4$); 2) the CFH algorithm (Alg-YA) exhibits a $P_f > 10^{-4} (P_f > 10^{-3})$ for L > 5; 3) the CSFEC and HCSFEC algorithms are substantially more robust than all the other algorithms since are characterized by a $P_f < 10^{-6}$ for $L \le 8$; and 4) the HCSFEC is slightly outperformed by the CSFEC for L=10. Once again, the price to be paid for a lower probability of failure is represented by a larger computational effort. For instance, if L = 6, the CT required by the CSFEC (HCSFEC) algorithm is about 50 (4) times larger than that characterizing the CFH algorithm.

Finally, let us focus on **S5**. In this case, the performance index RMSE_f has been evaluated for the normalized frequencies of all the tones; moreover, six different values of the tone spacing $(\Delta F \cdot N)$ have been considered. Our

TABLE II
Signal-to-Noise Ratio Characterizing Each Tone in the Fifth Scenario and Corresponding CRLB
Evaluated for the Estimation of Its Frequency

	T1	T2	Т3	T4	T5	Т6	T7	Т8	Т9	T10
SNR (dB) CRLB (dB)										

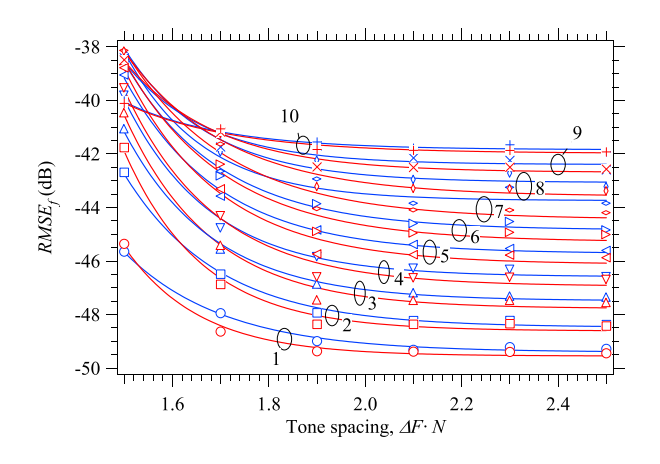


Fig. 8. RMSE performance achieved in frequency estimation versus tone separation (fifth scenario). The CSFEC (blue curves) and HCSFEC (red curves) algorithms are considered. Different tones are identified by distinct markers and numbers.

numerical results refer to the CSFEC and the HCSFEC algorithms only since we found that these are the only algorithms operating above their thresholds for spacings greater than 2/N. The CFH algorithm, the Alg-S, the Alg-YA, and the Alg-DP, instead, are characterized by a high probability of failure (more specifically, $P_f > 10^{-2}$ in all the conditions) and, as a matter of fact, are unable to detect all the tones and/or to accurately estimate their parameters. The dependence of $RMSE_f$, obtained under the assumption that SNR = 10 dB for the strongest tone [i.e., for the tone having the smallest frequency; see (49)], on $(\Delta F \cdot N)$ is illustrated in Fig. 8, whereas the values of the SNR and the CRLB referring to each of the ten tones are listed in Table II. Our results lead easily to the following conclusions: 1) the $RMSE_f$ characterizing the HCSFEC algorithm is lower than that achieved by the CSFEC algorithm for each tone and for all the values of tone spacing, since the last algorithm suffers from a larger (even if really limited) bias; 2) weaker tones are characterized by a larger RMSE_f (but also by a larger value of the CRLB, since their SNR is lower) for any ΔF ; 3) the RMSE_f characterizing each tone reaches a floor for $\Delta F > 2/N$; and 4) the floor appearing in the frequency estimation accuracy of each tone is very close to the CRLB evaluated for that tone.

B. Numerical Results Based on Experimental Measurements

The accuracy of the proposed CSFEC and HCSFEC algorithms has also been assessed on the basis of a real dataset acquired through a commercial MIMO radar. In particular, a

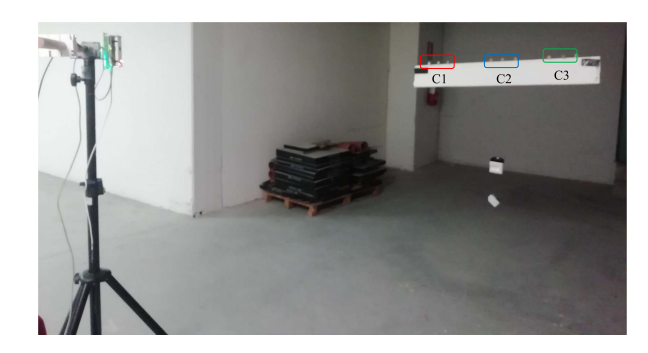


Fig. 9. Experimental setup developed for our acquisitions. The employed radar device is mounted on a wooden bar; the targets are small coins placed on a polystyrene plate.

measurement campaign has been accomplished in the building of our institution to acquire a dataset through a colocated FMCW MIMO radar operating in the E-band. The employed device is the TIDEP-01012 cascade mmWave radar; it is manufactured by Texas Instrument, Inc. [62] and classified as a long range radar. Its main parameters are: 1) chirp rate $\mu = 6.5 \times 10^{13} \text{ Hz/s}$; 2) bandwidth B = 4.1GHz; 3) central frequency $f_0 = 77$ GHz; 4) sampling frequency $f_s = 8$ MHz; and 5) number of samples per chirp N = 512. Moreover, it is endowed with a planar array made of $N_T = 12$ TX antennas and $N_R = 16$ RX antennas; each of its antennas consists of an array of four patch antennas. In principle, $12 \times 16 = 192$ virtual antennas are available in this case; however, only 86 horizontal-aligned and equally spaced virtual antennas, forming a virtual uniform linear array (ULA) with interantenna spacing $d_{\rm H} = \lambda/4$, have been exploited in our work.⁸ This choice allows us to achieve the range resolution $\Delta R = c/(2B) = 3.6$ cm and the azimuthal resolution $\Delta \theta = 1.35^{\circ}$.

All the measurements have been acquired in a large empty room (whose width, depth, and height are 10, 8, and 2.5 m, respectively). The radar device has been mounted on an horizontal wooden bar and has been lifted by a tripod at a height of roughly 1.60 m from the ground (see Fig. 9).

In our experimental setup, a pico flexx camera manufactured by PMD Technologies, Inc. [64] has been employed as a *reference sensor*; this device is based on a near-infrared vertical cavity surface emitting laser and is able to provide a depth map or, equivalently, a 3-D point cloud of a small region of the observed environment (its maximum depth is equal to 4 m, whereas its *field of view* is $62^{\circ} \times 45^{\circ}$).

⁸Further details about the adopted radar system and its physical and virtual arrays can be found in [63], Par. X.B].

TABLE III

Exact Position (Range and Azimuth) of Each of the Nine Targets Characterizing the Sixth Scenario

Me	thod	T_1	T_2	Т3	T_4	T_5	T ₆	T ₇	T ₈	T ₉
Exact	R (m)	1.755	1.780	1.816	1.950	2.010	2.057	2.195	2.254	2.280
Exact	θ (°)	-5.5	- 4.1	-2.7	3.1	4.6	6.0	9.1	10.3	11.5
CSFEC	\hat{R} (m)	1.801	1.834	1.853	2.013	2.064	2.094	2.193	2.248	2.299
(M=4)	$\bar{\varepsilon}_{\psi}$ (rad)	1.228	1.310	2.161	3.066	1.836	3.019	3.863	2.026	4.329
HCSFEC	R (m)	1.801	1.833	1.853	2.012	2.062	2.094	2.193	2.250	2.290
(M=4)	$\bar{\varepsilon}_{\psi}$ (rad)	1.162	1.336	2.064	3.027	1.836	3.021	3.873	2.053	3.262
CSFEC	\hat{R} (m)	1.809	1.840	1.861	2.007	2.053	2.094	2.196	2.249	2.298
(M=1)	$\bar{\varepsilon}_{\psi}$ (rad)	1.879	2.649	2.856	2.456	2.131	4.362	3.444	3.472	3.496
HCSFEC	R (m)	1.808	1.839	1.860	2.006	2.058	2.093	2.193	2.249	2.301
(M=1)	$\bar{\varepsilon}_{\psi}$ (rad)	2.960	2.710	1.795	1.864	3.070	4.299	4.430	1.976	4.234
CFH	\hat{R} (m)	1.795	1.825	1.854	1.875	2.008	2.055	2.092	2.250	2.301
CITI	$\bar{\varepsilon}_{\psi}$ (rad)	1.413	1.293	2.126	2.849	2.555	2.015	3.991	3.321	2.119
Alg-YA	\hat{R} (m)	1.787	1.854	1.875	1.875	2.012	2.067	2.090	2.190	2.289
Aig-1A	$\bar{\varepsilon}_{\psi}$ (rad)	1.294	4.020	2.891	2.364	2.123	4.243	3.930	2.152	2.485
Λ1α \$	\hat{R} (m)	1.809	1.809	1.809	1.809	1.809	1.809	1.822	1.837	2.204
Alg-S	$\bar{\varepsilon}_{\psi}$ (rad)	0.965	1.311	2.097	2.966	2.428	3.088	4.037	4.193	3.200
Alg-DP	\hat{R} (m)	1.843	1.854	1.855	1.856	1.856	1.857	1.865	1.867	2.204
Alg-DP	$\bar{\varepsilon}_{\psi}$ (rad)	3.161	2.635	3.360	3.260	4.691	3.243	5.572	3.207	6.316

The range estimates computed by the Alg-YA, the Alg-DP, and the CSFEC, HCSFEC, and CFH algorithms are listed. Moreover, the phase RMSE computed for each target is provided.

As far as the acquired measurements are concerned, it is important to point out that: 1) all the target ranges have been estimated with respect to the central virtual channel of the ULA; 2) the exact target positions have been acquired with respect to the center of the pico flexx camera. Therefore, in comparing these positions with their estimates computed on the basis of the radar measurements, the distance $\Delta_{FP}=33\,\mathrm{cm}$ between the FMCW radar and the camera was always kept into account; and 3) all our measurements have been processed in the MATLAB environment (running on a desktop computer equipped with an i7 processor).

The numerical results illustrated in this paragraph refer to two static scenarios. The first scenario is denoted **S6** and is characterized by the presence of an overall number of targets ranging from 1 to 9 (so that $1 \le L \le 9$). As shown in Fig. 9, the targets, placed on a polystyrene plate, are represented by small coins, each having a diameter equal to 2 cm (note that such coins are grouped in three different clusters, called C1, C2, and C3); their exact positions are listed in Table III (the data referring to the *i*th target are collected in the column identified by T_i , with i = 1, 2, ..., 9). In the second scenario (denoted **S7**), instead, five distinct experiments, characterized by a different number of targets, have been conducted. The results obtained in this scenario have allowed us to assess how the performance of our

estimation algorithms is influenced by the overall number of targets (i.e., by L).

In processing all the acquired measurements, the prior knowledge of L has been always assumed and an oversampling factor M equal to 1 has been adopted for all the algorithms (namely, the CSFEC, HCSFEC, and CFH algorithms and the Alg-YA, the Alg-S, and the Alg-DP); moreover, M=4 has also been considered for the CSFEC and HCSFEC algorithms. The values of all the other parameters characterizing the considered estimation algorithms have been selected in the same way as the scenarios S2, S3, S4, and S5 described in the previous paragraphs.

In analyzing the data acquired in **S6** and **S7**, the accuracy of the *range* estimates evaluated for multiple targets has been assessed by evaluating the RMSE

$$\bar{\varepsilon}_R \triangleq \sqrt{\frac{1}{N_m} \sum_{l=0}^{N_m - 1} \left[R_l - \hat{R}_l \right]^2}$$
 (51)

and the peak error

$$\hat{\varepsilon}_R \triangleq \max_{l} \left| R_l - \hat{R}_l \right| \tag{52}$$

where N_m represents the overall number of available measurements. As far as the estimation of the complex amplitude characterizing the echo of a given target on a specific

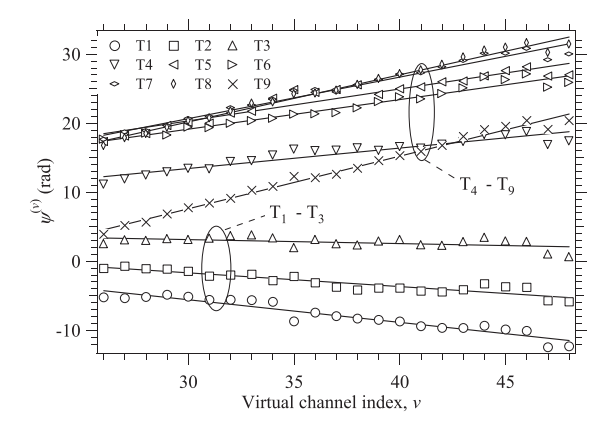


Fig. 10. Unwrapped phase of the complex gain associated with a given target versus the index of the virtual channel of the employed ULA; scenario S6 is considered.

virtual channel is concerned, it is important to point out that the RCS of the targets detected in our experiment was unknown. For this reason, our analysis of the complex gains estimated over the 86 channels of the available virtual ULA and associated with each target has concerned only their (unwrapped) phase. The phases estimated by the CSFEC algorithm over the above-mentioned ULA and associated with the nine targets of **S6** are shown in Fig. 10. Since the distance $d_{\rm H}$ between adjacent virtual channels is constant, the estimated phases exhibit a linear dependence on the index of the virtual channel (see [63], (10) and (11)]). Moreover, if a linear fitting is drawn for these data, it should be expected that the slope of the resulting lines is proportional to $\sin(\theta)$, where θ is the azimuth of the considered target (see [63], (23)]); this is confirmed by the results shown in Fig. 10, where the three (six) lines associated with the targets T_1-T_3 (T_4-T_9) have a negative (positive) slope, 9 as should be expected on the basis of Table III. To assess the quality of the estimated phases, their RMSE $\bar{\epsilon}_{\psi}$ has been evaluated on the basis of a formula similar to (51) (in this case, N_m represents the overall number of virtual channels for which the estimates of the phases associated with a given target have been computed); in doing so, the linear fitting of the phases estimated over the whole ULA has been taken as a reference with respect to which phase errors have been

The estimates of the target range generated by all the considered estimation algorithms for each of the targets of **S6** are listed in Table III; in the same table, the value of the phase RMSE $\bar{\epsilon}_{\psi}$ computed for each target is also provided. The numerical results collected in this table have also been processed to compute: 1) the errors $\bar{\epsilon}_R$ (51) and $\hat{\epsilon}_R$ (52); 2) the average errors $\bar{\epsilon}_{m,R}$ and $\hat{\epsilon}_{m,R}$ (these represent the average of $\bar{\epsilon}_R$ and $\hat{\epsilon}_R$, respectively, over the whole virtual ULA¹⁰); 3) the average of $\bar{\epsilon}_{\psi}$, denoted $\bar{\epsilon}_{m,\psi}$ (this represents the average

TABLE IV

Range RMSE $\bar{\varepsilon}_R$ (and Its Average $\bar{\varepsilon}_{m,R}$), Phase RMSE $\bar{\varepsilon}_{m,\psi}$, Range Peak Error $\hat{\varepsilon}_R$ (and Its Average $\hat{\varepsilon}_{m,R}$), and CT Evaluated for All the Considered Estimation Algorithms; the Sixth Scenario Is Considered

Method	$\bar{\varepsilon}_R$ (m)	$ar{arepsilon}_{m,R}$ (m)	$\hat{arepsilon}_R$ (m)	$\begin{array}{c} \hat{\varepsilon}_{m,R} \\ (\mathrm{m}) \end{array}$	$ar{arepsilon}_{m,\psi}$ (rad)	CT (second)
CSFEC $(M=4)$	0.04	0.05	0.06	0.11	2.80	0.030
HCSFEC $(M=4)$	0.04	0.05	0.06	0.11	2.80	0.030
CSFEC $(M=1)$	0.04	0.05	0.06	0.12	2.90	0.020
HCSFEC $(M=1)$	0.04	0.05	0.06	0.12	3.0	0.020
CFH	0.05	0.07	0.10	0.12	2.60	0.010
Alg-YA	0.06	0.07	0.10	0.14	2.60	0.040
Alg-S	0.30	0.11	0.40	0.19	3.50	0.050
Alg-DP	0.20	0.15	0.40	0.61	2.90	0.005

of the N_m values available for $\bar{\varepsilon}_{\psi}$); and 4) the CT. The values of all these performance indices are summarized in Table IV for the six considered estimation algorithms.

From the last results and those listed in Table III, the following conclusions can be drawn.

- 1) Both the CSFEC and HCSFEC algorithms are able to generate accurate estimates of the range and the amplitude of all the given targets for both the considered values of the oversampling factor *M*.
- 2) The values of range RMSE $\bar{\epsilon}_R$ and peak error $\hat{\epsilon}_R$ characterizing the CSFEC and HCSFEC algorithms are lower than those provided by all the other algorithms. In particular, even if the values of the range RMSE obtained by the CFH and Alg-YA are quite close to those of the CSFEC and HCSFEC algorithms, the peak errors of the first two algorithms are higher than the minimum range resolution allowed by the employed radar device and are two times larger than those characterizing the last two algorithms. Moreover, the range RMSE and peak errors of the CSFEC and HCSFEC algorithms are much lower those of the Alg-S and the Alg-DP. This result is due to the fact that the ranges estimated by the Alg-S and the Alg-DP are far from their true values, as it can be easily inferred from Table III.
- 3) The values of the range average errors $\bar{\epsilon}_{m,R}$ and $\hat{\epsilon}_{m,R}$ exhibit the same trend as $\bar{\epsilon}_R$ and $\hat{\epsilon}_R$, respectively, but are higher than the range RMSE and range peak error, respectively, obtained for the central channel of our virtual ULA. Note also that the large values of $\hat{\epsilon}_{m,R}$ and $\hat{\epsilon}_{m,R}$ found for the Alg-S and the Alg-DP are due to the fact that these algorithms do not converge in the considered scenario.
- 4) The values of the phase average RMSE $\bar{\epsilon}_{m,\psi}$ evaluated for the CSFEC and HCSFEC algorithms are comparable with (much lower that) those obtained for the CFH and the Alg-YA (the Alg-S and the Alg-DP).

 $^{^9\}mathrm{The}$ phase trajectories shown in Fig. 10 refer to a small portion of the available virtual ULA for better readability.

¹⁰In this case, the range estimate \hat{R}_l appearing in (51) and (52) is computed for each channel of the given virtual ULA, while the true value R_l is kept constant along this array.

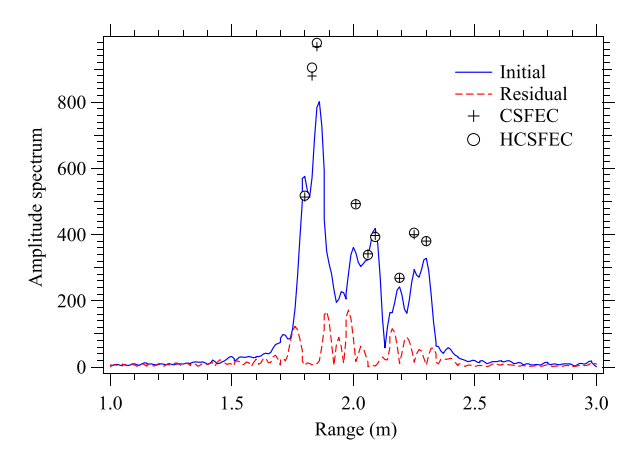


Fig. 11. Representation of the initial amplitude spectrum of the signal observed on the central virtual channel (blue line) and of the final *residual* amplitude spectrum generated by the CSFEC algorithm (red line). The range and the amplitude characterizing the nine targets of the sixth scenario and estimated by the CSFEC (HCSFEC) algorithm are indicated by black crosses (circles); *M* = 4 is assumed.

5) The CTs are in the order of few milliseconds for all the algorithms; the best tradeoff between accuracy and CT is achieved by the CSFEC and HCSFEC algorithms with an oversampling factor equal to 1. Note also that the fastest algorithm is represented by the Alg-DP, but its estimation accuracy is significantly worse than that provided by the CSFEC and HCSFEC algorithms.

It is also important to point out that the robustness of the CSFEC and HCSFEC algorithms is related to the accuracy of the estimation and cancellation procedure they accomplish. This is exemplified by Fig. 11, where the *initial amplitude spectrum* of the signal received on the central virtual channel in the sixth scenario and *its residual*, resulting from the cancellation of the spectral contributions due to the nine targets, are shown. Moreover, the range and the amplitude estimated by the CSFEC and HCSFEC algorithms for each target are shown (M = 4 is assumed).

Let us focus on **S7** now. The exact positions of the targets characterizing our five experiments are listed in Table V. In this case, L ranges from five to ten; note also that T $_l$ denotes the l th target (with l = 1, 2, ..., 10).

The values of the range RMSE $\bar{\epsilon}_R$ and peak error $\hat{\epsilon}_R$ obtained for all the considered estimation algorithms are listed in Tables VI and VII, respectively. The values of the range average errors $\bar{\epsilon}_{m,R}$ and $\hat{\epsilon}_{m,R}$ evaluated by averaging the RMSE $\bar{\epsilon}_R$ and the peak error $\hat{\epsilon}_R$ obtained for the central channel in all our experiments and the average CT are listed in Table VIII. From these results, the following points are derived.

 The ability of the CSFEC and HCSFEC algorithms in estimating the range of multiple targets becomes evident when the overall number of targets L increases. In fact, as evidenced by the numerical results collected in Tables VI and VII, the CSFEC and HCSFEC algorithms achieve the lowest RMSE and

TABLE V

Exact Positions of the Targets Characterizing the Seventh Scenario;
Five Different Experiments Are Considered

Exp.	Exact #1 (m)	Exact #2 (m)	Exact #3 (m)	Exact #4 (m)	Exact #5 (m)
T_1	1.775	1.832	1.798	1.755	1.755
T_2	1.876	1.920	1.832	1.780	1.780
T ₃	2.003	1.930	1.920	1.816	1.816
T ₄	2.145	1.981	1.930	1.950	1.950
T ₅	2.228	2.055	1.981	2.010	2.010
T ₆		2.100	2.055	2.057	2.057
T ₇		2.220	2.100	2.195	2.195
T ₈			2.220	2.254	2.254
T ₉				2.280	2.280
T ₁₀					2.310

TABLE VI Range RMSE $\bar{\epsilon}_R$ Evaluated for All Our Experiments; the Seventh Scenario Is Considered

Method	Exp. 1 (m)	Exp. 2 (m)	Exp. 3 (m)	Exp. 4 (m)	Exp. 5 (m)
CSFEC $(M=4)$	0.06	0.03	0.04	0.04	0.06
HCSFEC $(M=4)$	0.06	0.03	0.04	0.04	0.06
CSFEC $(M=1)$	0.06	0.05	0.04	0.04	0.06
$\overline{\text{HCSFEC } (M=1)}$	0.06	0.05	0.04	0.04	0.06
CFH	0.06	0.05	0.04	0.05	0.07
Alg-YA	0.07	0.05	0.04	0.06	0.08
Alg-S	0.07	0.07	0.07	0.30	0.14
Alg-DP	0.07	0.12	0.07	0.20	0.22

TABLE VII
Range Peak Error $\hat{\epsilon}_R$ Evaluated for All Our Experiments; the Seventh
Scenario Is Considered

Method	Exp. 1 (m)	Exp. 2 (m)	Exp. 3 (m)	Exp. 4 (m)	Exp. 5 (m)
CSFEC $(M=4)$	0.12	0.06	0.06	0.06	0.13
$\overline{\text{HCSFEC } (M=4)}$	0.12	0.06	0.06	0.06	0.13
CSFEC $(M=1)$	0.12	0.10	0.05	0.06	0.13
HCSFEC (M = 1)	0.12	0.10	0.05	0.06	0.13
CFH	0.12	0.13	0.08	0.10	0.15
Alg-YA	0.12	0.15	0.05	0.10	0.21
Alg-S	0.12	0.13	0.14	0.40	0.24
Alg-DP	0.12	0.24	0.10	0.40	0.37

peak errors in all the experiments for both the values of M.

2) All the considered algorithms achieve comparable accuracies in the first experiment, i.e., when L=5. In the experiments characterized by L>5, the CSFEC and HCSFEC algorithms achieve the lowest

TABLE VIII

Average RMSE $\bar{\varepsilon}_{m,R}$, Peak Error $\hat{\varepsilon}_{m,R}$, and CT

Evaluated in the Seventh Scenario

Method	$ar{arepsilon}_{m,R}$ (m)	$\begin{array}{c} \hat{\varepsilon}_{m,R} \\ (\mathrm{m}) \end{array}$	CT (sec)
$\overline{\text{CSFEC } (M=4)}$	0.04	0.08	0.020
$\overline{\text{HCSFEC } (M=4)}$	0.04	0.08	0.020
$\overline{\text{CSFEC } (M=1)}$	0.05	0.09	0.010
$\overline{\text{HCSFEC } (M=1)}$	0.05	0.09	0.010
CFH	0.06	0.11	0.010
Alg-YA	0.06	0.13	0.060
Alg-S	0.13	0.21	0.060
Alg-DP	0.14	0.24	0.005

peak errors for both the values of M. Moreover, the errors significantly increase for Alg-S and Alg-DP when L > 8 (i.e., in experiments 4 and 5).

3) The average CT achieved by the CSFEC and HCS-FEC algorithms is comparable with those of the other algorithms (for example, the average CT of the CSFEC and HCSFEC algorithms for M=1 is equal to that of the CFH algorithm); however, the estimation accuracy they achieve is higher.

V. CONCLUSION

In this article, an algorithm for detecting and estimating a single tone was derived; moreover, it was shown how it can be exploited to estimate multiple tones through a serial cancellation procedure. The accuracy and robustness of the devised single-tone and multiple-tone estimators were assessed by means of extensive computer simulations involving both synthetically generated data and the measurements acquired through a commercial colocated MIMO FMCW radar. Our results evidenced that our multiple-tone estimators outperform all the other related estimators available in the technical literature in terms of the probability of convergence and accuracy when they operate in the presence of multiple closely spaced tones. For this reason, if they are employed in FMCW radar systems, they allow us to achieve excellent range resolution and to acquire direction of arrival information from the phase estimates computed on an antenna array. Future work concerns the application of the developed algorithms to various fields.

APPENDIX A A. SPECTRUM CANCELLATION

In this appendix, the expression of the vector $\bar{\mathbf{C}}_0(\hat{A}_l[r-1], \hat{F}_l[r-1])$ appearing in the RHS of (40) is derived. The vector $\bar{\mathbf{C}}_0(\cdot, \cdot)$ is evaluated to cancel the contribution of the sequence [see (3)]

$$s_n(\bar{F}_l, \bar{A}_l) \triangleq \bar{A}_l \exp(j2\pi n\bar{F}_l) = \bar{A}_l \bar{w}_l^n$$
 (53)

to the vector \mathbf{X}_0 (12); here, $\bar{w}_l \triangleq \exp(j2\pi \bar{F}_l)$. Since \mathbf{X}_0 is the N_0 th-order DFT of the zero-padded vector $\mathbf{x}_{0,\text{ZP}}$ (13)

(where the vector \mathbf{x}_0 collects the elements of the complex sequence $\{x_n; n=0, 1,..., N-1\}$), it can be shown that $\bar{\mathbf{C}}_0(\hat{A}_l[r-1], \hat{F}_l[r-1]) = \bar{A}_l \ \bar{\mathbf{W}}_0^{(l)}$, where $\bar{\mathbf{W}}_0^{(l)}$ denote the N_0 th-order DFT of the vector $\bar{\mathbf{w}}_0^{(l)} \triangleq [1, \bar{w}_l, \bar{w}_l^2, ..., \bar{w}_l^{N-1}, 0,..., 0]^T$. Then, the mth element of the vector $\bar{\mathbf{W}}_0^{(l)}$ is given by

$$\bar{W}_{0}^{(l)}[m] = \frac{1}{N_{0}} \sum_{n=0}^{N-1} \bar{w}_{l}^{n} \exp\left(-j\frac{2\pi m}{N_{0}}n\right)$$

$$= \frac{1}{N_{0}} \sum_{n=0}^{N-1} (q[m])^{n}$$
(54)

where $\hat{q}[m] \triangleq \exp(j2\pi(\hat{F} - m/N_0))$. Therefore, the identity

$$\sum_{n=0}^{N-1} q^n = \frac{q^N - 1}{q - 1} \tag{55}$$

holding for any $q \in \mathbb{C}$ can be exploited for an efficient computation of all the elements of the vector $\bar{\mathbf{W}}_0^{(l)}$.

APPENDIX B LEAKAGE CANCELLATION

In this appendix, the expression of the quantity $\bar{X}_{lk,k}(\hat{A}_l[r-1],\hat{F}_l[r-1],\hat{F}_{c,r}[r])$ appearing in the RHS of (43) and (45) is derived for the CSFEC algorithm. This quantity is computed to cancel the contribution of the sequence $\{s_n(\bar{F}_l,\bar{A}_l)\}$ (53) to $\bar{X}_{k,\rho[r]}$ for k=0,1,2,3. Since $\bar{X}_{k,\rho[r]}$ is defined by (20), it can be shown that

$$\bar{X}_{lk,k}(\hat{A}_{l}[r-1], \hat{F}_{l}[r-1], \hat{F}_{c,r}[r]) = \bar{A}_{l} \, \bar{W}_{k}^{(l)}(\hat{F}_{c,r}[r])$$
(56)

where

$$\bar{W}_{k}^{(l)}(\hat{F}_{c,r}[r]) = \frac{1}{N_0} \sum_{n=0}^{N-1} n^{k} \, \bar{w}_{l}^{n} \exp(-j2\pi n \hat{F}_{c,r}[r])$$

$$= \frac{1}{N_0} \sum_{n=0}^{N-1} n^{k} (\bar{q}[r])^{n}$$
(57)

and $\bar{q}[r] \triangleq \exp(j2\pi(\bar{F}_l - \hat{F}_{c,r}[r]))$. Therefore, the identities (55)

$$(q-1)^2 \sum_{n=0}^{N-1} n \, q^n = (N-1)q^{N+1} - Nq^N + q$$
 (58)

$$(q-1)^{3} \sum_{n=0}^{N-1} n^{2} q^{n} = (N-1)^{2} q^{N+2} + N^{2} q^{N} - q^{2} - q$$
$$- (2N^{2} - 2N - 1) q^{N+1}$$
 (59)

and

$$(q-1)^{4} \sum_{n=0}^{N-1} n^{3} q^{n} = q + 4q^{2} + q^{3} - N^{3} q^{N}$$

$$+ (3N^{3} - 3N^{2} - 3N - 1)q^{N+1}$$

$$+ (-3N^{3} + 6N^{2} - 4)q^{N+2}$$

$$+ (N-1)^{3} q^{N+3}$$
 (60)

can be exploited for an efficient computation of all the terms appearing in the RHS of (43) and (45), with k = 0, 1, 2, and 3.

REFERENCES

- S. M. Patole, M. Torlak, D. Wang, and M. Ali, "Automotive radars: A review of signal processing techniques," *IEEE Signal Process. Mag.*, vol. 34, no. 2, pp. 22–35, Mar. 2017.
- [2] T. Schmidl and D. Cox, "Robust frequency and timing synchronization for OFDM," *IEEE Trans. Commun.*, vol. 45, no. 12, pp. 1613–1621, Dec. 1997.
- [3] B. Fleury, M. Tschudin, R. Heddergott, D. Dahlhaus, and K. I. Pedersen, "Channel parameter estimation in mobile radio environments using the SAGE algorithm," *IEEE J. Sel. Areas Commun.*, vol. 17, no. 3, pp. 434–450, Mar. 1999.
- [4] Y. Baoguo, K. B. Letaief, R. S. Cheng, and Z. Cao, "Channel estimation for OFDM transmission in multipath fading channels based on parametric channel modeling," *IEEE Trans. Commun.*, vol. 49, no. 3, pp. 467–479, Mar. 2001.
- [5] P. Whittle, "The simultaneous estimation of a time series harmonic components and covariance structure," *Trabajos de Estadística*, vol. 3, no. 1, pp. 43–57, 1952.
- [6] A. M. Walker, "On the estimation of a harmonic component in a time series with stationary independent residuals," *Biometrika*, vol. 58, no. 1, pp. 21–36, 1971.
- [7] D. C. Rife and R. R. Boorstyn, "Multiple tone parameter estimation from discrete-time observations," *Bell Syst. Tech. J.*, vol. 55, no. 9, pp. 1389–1410, Nov. 1976.
- [8] M. Macleod, "Fast nearly ML estimation of the parameters of real or complex single tones or resolved multiple tones," *IEEE Trans. Signal Process.*, vol. 46, no. 1, pp. 141–148, Jan. 1998.
- [9] R. Schmidt, "Multiple emitter location and signal parameter estimation," *IEEE Trans. Antennas Propag.*, vol. 34, no. 3, pp. 276–280, Mar. 1986.
- [10] R. Roy and T. Kailath, "ESPRIT-estimation of signal parameters via rotational invariance techniques," *IEEE Trans. Acoust. Speech Signal Process.*, vol. 37, no. 7, pp. 984–995, Jul. 1989.
- [11] J. Capon, "High-resolution frequency-wavenumber spectrum analysis," *Proc. IEEE*, vol. 57, no. 8, pp. 1408–1418, Aug. 1969.
- [12] J. Li and P. Stoica, "An adaptive filtering approach to spectral estimation and SAR imaging," *IEEE Trans. Signal Process.*, vol. 44, no. 6, pp. 1469–1484, Jun. 1996.
- [13] T. Yardibi, J. Li, P. Stoica, M. Xue, and A. B. Baggeroer, "Source localization and sensing: A nonparametric iterative adaptive approach based on weighted least squares," *IEEE Trans. Aerosp. Electron. Syst.*, vol. 46, no. 1, pp. 425–443, Jan. 2010.
- [14] P. Gough, "A fast spectral estimation algorithm based on the FFT," *IEEE Trans. Signal Process.*, vol. 42, no. 6, pp. 1317–1322, Jun. 1994.
- [15] J. Li and P. Stoica, "Efficient mixed-spectrum estimation with applications to target feature extraction," *IEEE Trans. Signal Process.*, vol. 44, no. 2, pp. 281–295, Feb. 1996.
- [16] J. Rissanen, "A universal prior for integers and estimation by minimum description length," *Ann. Statist.*, vol. 11, no. 2, pp. 416–431, Jun. 1983.
- [17] D. C. Rife and G. A. Vincent, "Use of the discrete Fourier transform in the measurement of frequencies and levels of tones," *Bell Syst. Tech. J.*, vol. 49, no. 2, pp. 197–228, Feb. 1970.
- [18] B. Quinn, "Estimating frequency by interpolation using Fourier coefficients," *IEEE Trans. Signal Process.*, vol. 42, no. 5, pp. 1264–1268, May 1994.
- [19] B. Quinn, "Estimation of frequency, amplitude, and phase from the DFT of a time series," *IEEE Trans. Signal Process.*, vol. 45, no. 3, pp. 814–817, Mar. 1997.
- [20] E. Jacobsen and P. Kootsookos, "Fast, accurate frequency estimators [DSP Tips Tricks]," *IEEE Signal Process. Mag.*, vol. 24, no. 3, pp. 123–125, May 2007.

- [21] Ç. Candan, "A method for fine resolution frequency estimation from three DFT samples," *IEEE Signal Process. Lett.*, vol. 18, no. 6, pp. 351–354, Jun. 2011.
- [22] Ç. Candan, "Analysis and further improvement of fine resolution frequency estimation method from three DFT samples," *IEEE Signal Process. Lett.*, vol. 20, no. 9, pp. 913–916, Sep. 2013.
- [23] U. Orguner and Ç. Candan, "A fine-resolution frequency estimator using an arbitrary number of DFT coefficients," *Signal Process.*, vol. 105, pp. 17–21, Dec. 2014.
- [24] C. Yang and G. Wei, "A noniterative frequency estimator with rational combination of three spectrum lines," *IEEE Trans. Signal Process.*, vol. 59, no. 10, pp. 5065–5070, Oct. 2011.
- [25] X. Liang, A. Liu, X. Pan, Q. Zhang, and F. Chen, "A new and accurate estimator with analytical expression for frequency estimation," *IEEE Commun. Lett.*, vol. 20, no. 1, pp. 105–108, Jan. 2016.
- [26] L. Fan and G. Qi, "Frequency estimator of sinusoid based on interpolation of three DFT spectral lines," *Signal Process.*, vol. 144, pp. 52–60, Mar. 2018.
- [27] L. Fan, G. Qi, J. Xing, J. Jin, J. Liu, and Z. Wang, "Accurate frequency estimator of sinusoid based on interpolation of FFT and DTFT," *IEEE Access*, vol. 8, pp. 44373–44380, 2020.
- [28] D. Rife and R. Boorstyn, "Single tone parameter estimation from discrete-time observations," *IEEE Trans. Inf. Theory*, vol. IT-20, no. 5, pp. 591–598, Sep. 1974.
- [29] T. Abatzoglou, "A fast maximum likelihood algorithm for frequency estimation of a sinusoid based on Newton's method," *IEEE Trans. Acoust., Speech, Signal Process.*, vol. ASSP-33, no. 1, pp. 77–89, Feb. 1985.
- [30] Y. V. Zakharov and T. C. Tozer, "Frequency estimator with dichotomous search of periodogram peak," *Electron. Lett.*, vol. 35, no. 19, pp. 1608–1609, Sep. 1999.
- [31] E. Aboutanios, "A modified dichotomous search frequency estimator," *IEEE Signal Process. Lett.*, vol. 11, no. 2, pp. 186–188, Feb. 2004.
- [32] E. Aboutanios and B. Mulgrew, "Iterative frequency estimation by interpolation on Fourier coefficients," *IEEE Trans. Signal Process.*, vol. 53, no. 4, pp. 1237–1242, Apr. 2005.
- [33] E. Aboutanios, "Estimating the parameters of sinusoids and decaying sinusoids in noise," *IEEE Instrum. Meas. Mag.*, vol. 14, no. 2, pp. 8–14, Apr. 2011.
- [34] Y. Liu, "Generalization of iterative Fourier interpolation algorithms for single frequency estimation," *Digit. Signal Process.*, vol. 21, no. 1, pp. 141–149, Jan. 2011.
- [35] I. Djurovic, "Estimation of the sinusoidal signal frequency based on the marginal median DFT," *IEEE Trans. Signal Process.*, vol. 55, no. 5, pp. 2043–2051, May 2007.
- [36] J.-R. Liao and C.-M. Chen, "Analysis and reduction of estimation bias for an iterative frequency estimator of complex sinusoid," in *Proc. IEEE Int. Conf. Acoust., Speech, Signal Process.*, 2013, pp. 6138–6142.
- [37] J.-R. Liao and S. Lo, "Analytical solutions for frequency estimators by interpolation of DFT coefficients," *Signal Process.*, vol. 100, pp. 93–100, Jul. 2014.
- [38] Y. V. Zakharov, V. M. Baronkin, and T. C. Tozer, "DFT-based frequency estimators with narrow acquisition range," *Proc. Inst. Elect. Eng.—Commun.*, vol. 148, no. 1, pp. 1–7, Feb. 2001.
- [39] C.-F. Huang, H.-P. Lu, and W.-H. Chieng, "Estimation of single-tone signal frequency with special reference to a frequency-modulated continuous wave system," *Meas. Sci. Technol.*, vol. 23, no. 3, Mar. 2012, Art. no. 035002.
- [40] S. Ye and E. Aboutanios, "An algorithm for the parameter estimation of multiple superimposed exponentials in noise," in *Proc. IEEE Int. Conf. Acoust., Speech, Signal Process.*, 2015, pp. 3457–3461.
- [41] S. Ye and E. Aboutanios, "Rapid accurate frequency estimation of multiple resolved exponentials in noise," *Signal Process.*, vol. 132, pp. 29–39, Mar. 2017.
- [42] A. Serbes and K. Qaraqe, "A fast method for estimating frequencies of multiple sinusoidals," *IEEE Signal Process. Lett.*, vol. 27, pp. 386–390, 2020.

- [43] A. Serbes, "Fast and efficient estimation of frequencies," *IEEE Trans. Commun.*, vol. 69, no. 6, pp. 4054–4066, Jun. 2021.
- [44] S. Djukanović and V. Popović-Bugarin, "Efficient and accurate detection and frequency estimation of multiple sinusoids," *IEEE Access*, vol. 7, pp. 1118–1125, 2019.
- [45] J. A. Hogbom, "Aperture synthesis with non-rectangular distribution of interferometric baselines," *Astron. Astrophys. Suppl.*, vol. 15, no. 3, pp. 417–426, Jun. 1974.
- [46] D. Zankl, S. Schuster, R. Feger, and A. Stelzer, "What a blast!: A massive MIMO radar system for monitoring the surface in steel industry blast furnaces," *IEEE Microw. Mag.*, vol. 18, no. 6, pp. 52–69, Sep./Oct. 2017.
- [47] E. Sirignano, A. Davoli, G. M. Vitetta, and F. Viappiani, "A comparative analysis of deterministic detection and estimation techniques for MIMO SFCW radars," *IEEE Access*, vol. 7, pp. 129848–129861, 2019
- [48] A. Serbes, "Fast and efficient sinusoidal frequency estimation by using the DFT coefficients," *IEEE Trans. Commun.*, vol. 67, no. 3, pp. 2333–2342, Mar. 2019.
- [49] T. Grandke, "Interpolation algorithms for discrete Fourier transforms of weighted signals," *IEEE Trans. Instrum. Meas.*, vol. IM-32, no. 2, pp. 350–355, Jun. 1983.
- [50] M. Macleod, "Fast DFT-domain algorithms for near-optimal tonal detection and frequency estimation," *Inst. Acoust. Proc.*, vol. 13, pp. 102–109, 1991.
- [51] D. Belega and D. Petri, "Sine-wave parameter estimation by interpolated DFT method based on new cosine windows with high interference rejection capability," *Digit. Signal Process.*, vol. 33, pp. 60–70, Oct. 2014.
- [52] K. Duda, L. B. Magalas, M. Majewski, and T. P. Zielinski, "DFT-based estimation of damped oscillation parameters in low-frequency mechanical spectroscopy," *IEEE Trans. Instrum. Meas.*, vol. 60, no. 11, pp. 3608–3618, Nov. 2011.
- [53] M. Feder and E. Weinstein, "Parameter estimation of superimposed signals using the EM algorithm," *IEEE Trans. Acoust., Speech, Signal Process.*, vol. 36, no. 4, pp. 477–489, Apr. 1988.
- [54] J. Fessler and A. Hero, "Space-alternating generalized expectation-maximization algorithm," *IEEE Trans. Signal Process.*, vol. 42, no. 10, pp. 2664–2677, Oct. 1994.
- [55] J. Selva, "ML estimation and detection of multiple frequencies through periodogram estimate refinement," *IEEE Signal Process. Lett.*, vol. 24, no. 3, pp. 249–253, Mar. 2017.
- [56] J. Li and P. Stoica, "MIMO radar with colocated antennas," *IEEE Signal Process. Mag.*, vol. 24, no. 5, pp. 106–114, Sep. 2007.
- [57] M. A. Richards, Fundamentals of Radar Signal Processing. New York, NY, USA: McGraw-Hill, 2005.
- [58] I. Ziskind and M. Wax, "Maximum likelihood localization of multiple sources by alternating projection," *IEEE Trans. Acoust., Speech, Signal Process.*, vol. 36, no. 10, pp. 1553–1560, Oct. 1988.
- [59] P. Di Viesti, A. Davoli, G. Guerzoni, and G. M. Vitetta, "Novel methods for approximate maximum likelihood estimation of multiple superimposed undamped tones and their application to radar systems," Jul. 2021. [Online]. Available: https://doi.org/10.36227/ techrxiv.15054321
- [60] J. Selva, "Efficient wideband DOA estimation through function evaluation techniques," *IEEE Trans. Signal Process.*, vol. 66, no. 12, pp. 3112–3123, Jun. 2018.
- [61] Y.-X. Yao and S. Pandit, "Cramer-Rao lower bounds for a damped sinusoidal process," *IEEE Trans. Signal Process.*, vol. 43, no. 4, pp. 878–885, Apr. 1995.
- [62] Imaging Radar Using Cascaded mmWave Sensor Reference Design—TIDEP-01012, Texas Instrum., Dallas, TX, USA, Accessed: Aug. 22, 2022. [Online]. Available: https://www.ti. com/tool/TIDEP-01012

- [63] P. Di Viesti, A. Davoli, G. Guerzoni, and G. M. Vitetta, "Novel deterministic detection and estimation algorithms for colocated multiple-input multiple-output radars," *IEEE Access*, vol. 10, pp. 2216–2255, 2022.
- [64] "Camboard pico flexx," Accessed: Aug. 22, 2022. [Online]. Available: https://pmdtec.com/picofamily/



Pasquale Di Viesti (Student Member, IEEE) received the bachelor's and master's degrees (*cum laude*) in electronic engineering from the University of Modena and Reggio Emilia, Modena, Italy, in 2016 and 2018, respectively, and the Ph.D. degree in automotive for an intelligent mobility from the University of Bologna, Bologna, Italy, in 2022.

He is currently a Postdoctoral Research Fellow with the University of Modena and Reggio Emilia. His main research interests include sta-

tistical signal processing and multiple-input multiple-output radars.



applications.

Alessandro Davoli (Student Member, IEEE) received the B.S. and M.S. (*cum laude*) degrees in electronic engineering from the University of Modena and Reggio Emilia, Modena, Italy, in 2016 and 2018, respectively.

He is currently a Postdoctoral Research Fellow with the University of Modena and Reggio Emilia. His main research interests include multiple-input multiple-output radars, with emphasis on the development of novel detection and estimation algorithms for automotive



Giorgio Guerzoni received the B.S. and M.S. degrees in electronic engineering in 2016 and 2019, respectively, from the University of Modena and Reggio Emilia, Modena, Italy, where he is currently working toward the Ph.D. degree in information and communication technology.

His main research interests include multipleinput multiple-output radars and machine learning, with emphasis on the development of novel detection and estimation algorithms.



Giorgio M. Vitetta (Senior Member, IEEE) received the Dr.Ing. (*cum laude*) degree in electronic engineering and the Ph.D. degree in information engineering from the University of Pisa, Pisa, Italy, in 1990 and 1994, respectively.

Since 2001, he has been a Full Professor of Telecommunications with the University of Modena and Reggio Emilia, Modena, Italy. He has coauthored more than 100 papers published on international journals and the proceedings of international conferences. He has coauthored the

book titled *Wireless Communications: Algorithmic Techniques* (Hoboken, NJ, USA: Wiley, 2013). His main research interests include wireless and wired data communications, localization systems, multiple-input multiple-output radars, and the smart grid.

Dr. Vitetta was an Area Editor for IEEE TRANSACTIONS ON COMMUNICATIONS and an Associate Editor for IEEE WIRELESS COMMUNICATIONS LETTERS and IEEE TRANSACTIONS ON WIRELESS COMMUNICATIONS.

Open Access provided by 'Università degli Studi di Modena e Reggio Emilia' within the CRUI CARE Agreement